The Canadian Journal of Mineralogy and Petrology
ISSN 2817-1713
Vol. 00, pp. 000-000 (2026)
DOI: 10.3749/2500062

CARBONATITE ANTISKARNS: A CRITICAL APPRAISAL

ROGER H. MITCHELL[§]

Department of Geology, Lakehead University, 955 Oliver Road, Thunder Bay, Ontario P7B 5E1, Canada

JOHN GITTINS

Department of Geology, University of Toronto, Toronto, Ontario M5S 3B1, Canada

FRANK J. SPERA

Department of Earth Science and Earth Research Institute, University of California, Santa Barbara, California 93106, USA

ABSTRACT

The antiskarn hypothesis considers that ultramafic rocks, such as pyroxenites, occurring in alkaline rock-carbonatite complexes, are formed by assimilative reactions between silica-free carbonatite-forming magma and solid silica-bearing country rocks. The geological, experimental, and thermodynamic evidence presented by proponents of the antiskarn process is examined critically, and it is concluded that carbonatite-forming magmas are not deficient in silica and typically crystallize abundant primary silicate minerals. Field and mineralogical evidence for antiskarn-formed rocks in most alkaline rock complexes is either absent, incorrectly interpreted, or of only local significance. Carbonatite-forming magmas can react with country rocks to form exoskarns (fenites) and minor ultramafic selvages (endoskarns) around silicate xenoliths and veins, but these reactions cannot result in the formation of voluminous silicate rocks present in alkaline rock-carbonatite complexes. The antiskarn reaction process is evaluated in terms of the enthalpies of 16 endothermic reactions and the thermal equilibration of granitic country rock when assimilated isenthalpically by carbonatite-forming magma by consideration of the relationship between the temperatures of post-mixing assemblages and the mass fractions of granite and carbonatite-forming magma endmembers. Calculations show that the large fractions of carbonatite-forming magma required to reach the solidus temperature of granitic country rock are not supported by field relations and that crystallization of the carbonatite-forming magma will occur before assimilation. It is concluded that there is no geological or thermodynamic evidence to support the antiskarn hypothesis.

Keywords: antiskarns, assimilation, carbonatite, pyroxenites, alkaline rocks.

INTRODUCTION

The antiskarn hypothesis as proposed by Anenburg & Mavrogenes (2018) and Anenburg *et al.* (2020) sought to explain the formation of the Nolans Bore REE-Th deposit (Australia), which consists of a series of near-monomineralic fluorapatite veins (meter-to-centimeter in width) with a diopside selvage emplaced in granitic country rocks. Although there is no geological evidence that carbonatite was ever present in this deposit, the authors declared that the deposit was formed from a "carbonatite magma" (*sic*). Note that the term "carbonatite magma" is never defined and is a commonly used colloquialism referring to what are actually carbonatite-forming magmas (see below).

As the principal evidence for the former presence of "carbonatite magma", it is stated by Anenburg *et al.* (2020, abstract p.1) that "sinusoidal REE distribution patterns in diopside, together with strong Yb-Lu enrichments relative to coexisting titanite, are suggestive of derivation from a Ce-rich carbonatite". Anenburg & Mavrogenes (2018) and Anenburg *et al*. (2020) consider that carbonatite-forming magmas react with their commonly silicic (granitic) host rocks, resulting in assimilation and incorporation of Si into Si-poor carbonatite-forming magma and the formation of silicate

[§] *Corresponding author e-mail address*: rmitchel@lakeheadu.ca

minerals in the intrusive carbonatite-forming magma. Such reaction-produced rocks are termed "antiskarns".

In a further discussion of the proposition, Anenburg & Walters (2024) argue that this explains the genesis of "silicocarbonatites", *i.e.*, rock in which silicates constitute more than 20 vol.% of the carbonatite. Central to the concept is the assumption that the SiO_2 content of "carbonatite magmas" (not defined) rarely exceeds 5 wt.% at crustal pressures (<1 GPa) "and are negligible at temperatures below 1000 °C" (Anenburg & Guzmics 2023). Consequently, an external source of SiO_2 must be found to explain how silicates can crystallize in the amounts commonly seen in carbonatite rocks. Antiskarn formation is held by Anenburg & Walters (2024) to be the answer to this conundrum.

Since the inception of the antiskarn concept, several authors (Vasyukova & Williams-Jones 2022, Vasyukova *et al.* 2022, Williams-Jones &Vasyukova 2023) have inappropriately extended the concept to explain the formation of all of the clinopyroxenites and glimmerites which occur in significant volumes in many carbonatite-alkaline rock complexes.

It is interesting to note that the antiskarn concept is essentially the inverse of the well-known "limestone assimilation" hypothesis proposed by Daly (1910). This hypothesis suggests that feldspathoidal rocks can be generated by the assimilation of limestone by granitic magma. We also note that the views of Anenburg and co-workers in some respects follow those of Holmes (1950) and Schuiling (1964), who postulated a "sial-syntexis hypothesis", in which a series of alkalic silicate rocks can be formed by assimilation of granite by "carbonatite magma". Both the sial-syntexis and limestone-syntexis hypotheses suffer from the same phase equilibria restrictions described by Wyllie & Watkinson (1970) and thermodynamic problems that render these processes improbable, as discussed further below.

Even before the introduction of the antiskarn concept, a number of examples of contamination of carbonatite-forming magma by assimilation of, or reaction with, silicate country rocks had been described. However, these all seem to be localized and there is no suggestion that this minor contamination has extensively altered the composition of large bodies of magma. For example, Chakhmouradian *et al*. (2008) note that at Eden Lake in Manitoba, Canada, "There is also abundant evidence for local assimilation of silicate material by carbonatite magma (*sic*) through xenolith digestion and wall rock reaction". This seems to be limited to the carbonatites near the silicate wall-rocks containing "abundant resorbed and fragmented xenocrysts of clinopyroxene and feldspars".

It is important to note that antiskarn formation is not equivalent to fenitization. Anenburg & Mavrogenes (2018) distinguish between *fenitized* rocks (or exoskarns), which are typically formed at the margins of carbonatite bodies by alkali-rich hydrothermal fluids expelled from the crystallizing magma as it approaches its solidus, and *antiskarns*, which are formed within a liquid "carbonatite magma" by virtue of its having reacted with, and assimilated, silica-rich country rocks.

Many articles describing carbonatite petrogenesis and antiskarn formation fail to distinguish between carbonatite rocks, carbonatite melts, and carbonatite magmas. These terms, which are *not* synonymous, are used interchangeably and commonly without definitions by the users. We note here that: (1) carbonatites are *rocks* consisting of primary igneous carbonates whose bulk compositions do not represent those of liquids; (2) carbonatite rocks are produced from diverse *carbonatite-forming magmas*; and (3) this latter term is NOT synonymous with the commonly used colloquial terms "carbonatite magma" or "carbonatite melt", as there are actually no actual "carbonatite magmas", there are only carbonatite-forming magmas; the term "carbonatite melt" should refer to the liquid component of a carbonatite-forming magma.

The Silica Content of Carbonatite-Forming Magmas

The overall assumption of many recent papers on the generation and evolution of carbonatite-forming magmas is that their silica content is insufficient to allow for the crystallization of the significant amounts of the common silicate minerals (amphibole, pyroxene, mica) present in carbonatite rocks. This observation forms the rationale of the antiskarn hypothesis that carbonatite-forming magmas are primary melts directly extracted from their mantle sources and not derived from carbonated silicate magmas. This approach is in direct contrast to petrogenetic studies of ijolite-carbonatite complexes, which are commonly considered to form from carbonated nephelinite magmas, *e.g.*, Napak (King 1949) and Prairie Lake (Savard & Mitchell 2021).

On the basis of some experiments and data from natural melt inclusions (Brooker & Kjarsgaard 2011, Weidendorfer *et al.* 2017, Yaxley *et al*. 2022, Schmidt *et al.* 2024), it has been concluded that the SiO_2 content of primary "carbonatite melts" does not exceed 5 wt.%. The higher SiO_2 contents of 15 wt.% reported by Berndt & Klemmer (2022) are considered by Anenburg & Guzmics (2023) to result from silicate melt contamination. However, in a synthesis of experimental data for natural and synthetic carbonated peridotite (Dasgupta *et al.* 2007; their Fig. 7) have shown that the silica contents of carbonated melts can range from about 2 to 50 wt.% SiO_2. From these data it is apparent that even "carbonatitic melts" can contain significant silica

contents (2–10 wt.% SiO_2). Thus, melts corresponding to carbonated silicate magmas, such as nephelinites or melilitites, can contain significant "carbonate" and silica contents, and that differentiation can lead to the formation of silica-bearing evolved carbonatite-forming magmas.

The antiskarn concept is based entirely on the assumption that the silica content of carbonatite-forming magmas is insufficient to form the amounts of silicate minerals commonly seen in carbonatites and other genetically related rocks (pyroxenites, ijolites *etc.*). Therefore, regardless of other geological and experimental evidence, it is postulated that an external source of silica must exist. An example of such reasoning is displayed by Bouabdellah *et al*. (2022), who noted that the silicate layers in the Twihinate complex have silica contents of 7–17 wt.% and therefore it is assumed that because the silica content of carbonatite-forming magmas must be far lower than this, there must be an external source for the Si, namely the felsic host rocks. Bouabdellah *et al*. (2022) conclude, without any further evidence, that assimilation of silicate wall-rocks is essential to producing the silica content necessary for the subsequent crystallization of the calc-silicate phases. A further example is provided by the Bayan Obo intrusion, where intrusion of carbonatite-forming magma into quartz conglomerate and quartz slate-sandstone has supposedly led to their desilication and metasomatic Na-fenite formation. Xiao *et al*. (2025) propose that, in addition, there is transfer of silica from the country rocks into the "carbonatite", which results in the formation of silicates in the carbonatite rocks. However, there is no actual evidence presented to support this hypothesis, as it is merely considered that the intruding "carbonatite magma" is *a priori* Si-poor and thus has insufficient silica activity to form silicates.

The commonly assumed Si and Al limits required by the antiskarn hypothesis are largely derived from melting experiments on carbonated common peridotite and eclogite compositions that produced carbonate-bearing melts as a direct consequence of doping the starting compositions with carbonates. We consider that for many of these studies the low assumed solubility values of Si and Al in carbonatites are based on an inadequate body of experimental bulk compositions. We contend, on the basis of the observed mineralogy of carbonatites, that the experiments underestimate both the silica and alumina contents of actual carbonatite-forming magmas.

It is particularly noteworthy that F was not present in any of the mantle melting experiments, and we suggest that its possible role has been overlooked. It is well established that fluorine is an important constituent of all carbonatite-forming magmas, as it is present in amphibole, phlogopite, and apatite, all of which appear to have crystallized throughout the evolution of most carbonatite-forming magmas. This observation suggests that fluorine

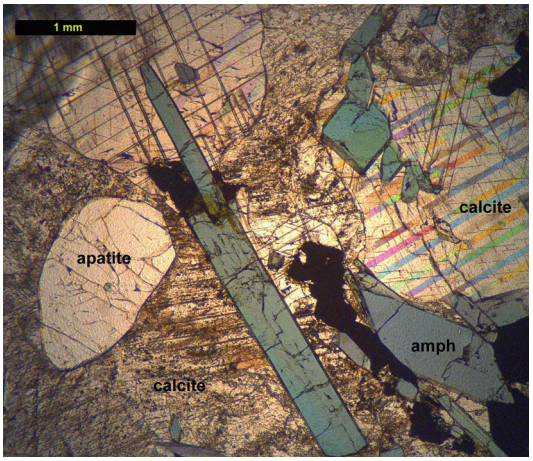

FIG. 1. Primary magnesio-arfvedsonite in calcite carbonatite, Cargill complex (Ontario). This is a typical example of the crystallization of primary liquidus amphibole from Si-bearing carbonatite magmas. Similar amphiboles are present in many carbonatites, *e.g.*, Argor, Seabrook Lake, Iron Hill, Panda Hill, Fen.

was present from the creation of the magma, not acquired at a later stage of evolution, and certainly not by antiskarn type reactions with F-poor country rocks. Indeed, phase equilibria studies on the join $CaCO_3$–CaF_2 demonstrate binary eutectic behavior with an invariant point eutectic at ~880 °C and $X_{CaF2} = 0.42$, indicative of high solubility of CaF_2 in molten $CaCO_3$ (Tomkute *et al*. 2014), consistent with the ubiquity of fluorite in carbonatites.

We suggest that the alleged silica problem is actually only a misapprehension. While it is clear that the compositions of carbonatite rocks are not necessarily those of the magma from which they crystallized, the fact remains that in many plutonic carbonatites their petrography indicates that silicate minerals are primary liquidus phases which have crystallized throughout the evolution of the magmas and display no evidence of cumulate disruption. These silicates show compositional variation from core-to-rim, suggesting they were generated from the silica originally present in the carbonatite-forming magma and that antiskarn reactions are not required for their origin. Examples of primary amphiboles such as that as illustrated in Figure 1 are to be found in many alkaline rock-carbonatite complexes.

Discussion of the Basis for the Antiskarn Process at Nolans Bore

The initial concept of antiskarn formation by Anenburg & Mavrogenes (2018) was an outgrowth of an attempt to explain REE transport by either hydrothermal or magmatic

processes rather than to introduce a general petrological concept. In support of their antiskarn contentions, Anenburg & Mavrogenes (2018) report a series of "sandwich" experiments in which layers of synthetic "carbonatite" (calcite+dolomite) and silico-granulite were reacted at temperatures of 400 and 900 °C and pressure of 0.6 GPa. The reactions resulted in the formation of fluorapatite together with diopside, forsterite, or wollastonite, thus simulating the diopsidic veins at the Nolans Bore deposit. The formation of diopside selvages was found to be dependent on the "carbonatite" composition, occurring *only* when the MgO/(CaO+MgO) ratio was approximately 0.2, with wollastonite or forsterite forming at lower or higher ratios, respectively. However, it would seem unlikely that natural processes would necessarily meet this condition. Subsequently, the authors restrict the alleged "carbonatite" responsible for the formation of Nolans Bore to a magnesian composition derived by partial melting of a "mantle source exceptionally enriched in P, and REE" to form a "magnesian carbonatite magma". They assume that ascent of "magnesian carbonatite magma" through the mantle results in reactions with enstatite to generate diopside and to become more "calcic" in the process. This resultant "carbonatitic liquid" is further assumed to have continued its ascent into the overlying silica-rich crust where it reacts to form diopside and produces clinopyroxenite. Subsequent erosion has exhumed fluorapatite-dominated veins and their diopsidic selvages to allow the proposed deduction, which is that "carbonatites, previously thought to be mostly unreactive, can undergo modification and modify the composition of the silicate rocks which they encounter, forming an 'antiskarn'." Note that Anenburg & Mavrogenes (2018 p. 361; their Fig. 10) restrict antiskarn formation to mid-crustal depths (>5 kb; 10–30 km), and that "normal" endo- and exoskarns form at shallow depths (<2 kb; <10 km). Clearly, this condition would seem to rule out any antiskarn formation in subvolcanic regimes, a restriction not considered by some recent adherents to the antiskarn hypothesis (Giebel *et al*. 2019, Walter *et al*. 2022, Su *et al*. 2023). Thus, Anenburg & Mavrogenes (2018) never actually proposed that the antiskarn concept was applicable to subvolcanic carbonatite-alkaline rock complexes.

Significant problems with the antiskarn hypothesis

There is no evidence for the presence of a carbonatite-forming magma at Nolans Bore.

The initial stages of the Anenburg & Mavrogenes (2018) antiskarn process are a development of the "mantle wehrlitization process" in which "dolomitic carbonatitic melts" are considered to traverse the lithospheric mantle in olivine and diopside rimmed conduits (Green & Wallace 1988). Interpretation of the experimental data of Dalton & Wood (1993) and Wyllie & Lee (1998) by Schmidt *et al.* (2024) shows that this process is thermodynamically impossible, as the reaction of "dolomite melt" with mantle minerals to become calcitic requires interaction with much colder lithosphere, a process resulting in heat loss and crystallization in the mantle. Any such reactions would be limited spatially due to the energetic constraints during approximately isenthalpic reaction.

Sinusoidal REE distribution patterns have been described for many mantle garnets and diopside (le Roux & Class 2016). The interpretation is always that metasomatism has introduced REE by Ca-bearing fluids which are always termed "carbonatites" even though these are actually hydrothermal or carbothermal fluids and no actual *bona fide* carbonatite is ever described. Much of this imprecise terminology essentially results in terming any carbonate-rich fluid or occurrence as "carbonatitic".

Anenburg & Mavrogenes (2018) confuse "carbonatite magmas", which are not defined, with fluids which are NOT magmas. In their "hydrothermal" experiments, these are fluids dominated by carbonate or bicarbonate anions and are actually carbohydrothermal fluids in terms of H_2O/CO_2 ratios. In the magmatic experiments there is reference to "liquid carbonatite", regardless that the experiments (650–900 °C; 6 kb) are all below the melting regimes of calcite or dolomite. Back-scattered electron images given by Anenburg & Mavrogenes (2018) show no equilibration, abundant subsolidus reactions related to carbonate decomposition and reactions with silicate, or quench features related to melting of the silicate component. Regardless, Anenburg & Mavrogenes (2018, p. 357) invoke "carbonatitic liquids" or "igneous carbonate patches" as the antiskarn forming agents and appear to consider that *bona fide* calcite or dolomite carbonatite bulk rock compositions represent those of liquids. This is impossible, as it is well-known that the bulk compositions of such carbonatites result from crystal accumulation. In conclusion, we can state with some confidence that the antiskarn hypothesis is a theoretical concept based on an interpretation of the genesis of the Nolans Bore REE-Th deposit from an assumed carbonatite-forming magma for which there is no geological evidence.

"Carbonatite Magma"-Mediated Metasomatism

Vasyukova & Williams-Jones (2022) and Williams-Jones & Vasyukova (2023) have invoked a metasomatic variant of the original sial-syntexis schemes of Holmes (1950) and von Eckermann (1950) to explain the origins of pyroxenites and phoscorites in some alkaline rock-carbonatite complexes. Although the process is not referred to by the proponents as an "antiskarn

process", it is clear that it is essentially a variant of this and therefore subject to the same thermodynamic problems (see below). The initial premise of Vasyukova & Williams-Jones (2022) and Williams-Jones & Vasyukova (2023) is that (1) carbonatite-forming magmas are the primary magmas for the formation of carbonatite-alkaline rock complexes, (2) pyroxenites and dunites cannot form by crystal fractionation processes from "mafic-to-ultramafic magmas (*sic*)" and that derivative rocks are not present in alkaline complexes, and (3) pyroxenites and dunites are metasomatic rocks. The model is essentially restricted to carbonatite-phoscorite intrusions surrounded by large volumes of ultramafic rocks. (Note that the use of the terms "mafic or ultramafic magma" is not correct, as these are petrographic terms which cannot be applied to liquids.)

It is proposed that repeated intrusion of veins, dikes, and plugs from millimeters to meters in diameter of magnesian carbonatite liquid (*sic*) reacts with the siliceous host rocks and results in the transfer of components (MgO and CaO) from the magma to the country rocks and the complete transformation of quartzo-feldspathic rock into ultramafic rocks such as glimmerites, clinopyroxenites, and peridotites/dunites. The metasomatism begins at the interface with the "carbonatitic magma" where thin films of diopside and forsterite form at the country rock contacts. With progressive magma-rock interaction the films thicken into wide monomineralic layers. Brittle fracturing of the country rocks and permeation of low viscosity carbonatite-forming magma is considered to be an essential component of the process which eventually sheaths the carbonatite veins with silicate minerals. The process results in a residual liquid enriched in Si, P, and Fe which evolves by crystallizing calcite until a phoscorite is produced. Vasyukova & Williams-Jones (2022) do not discuss either the free energy or enthalpy changes of the reactions proposed in their model; we discuss these below and show that these reactions are not realistic.

Problems with the carbonatite magma-mediated metasomatism hypothesis

It is assumed that parental "magnesio-carbonatitic magmas" are formed by extremely low degrees (<0.5 vol.%) of partial melting of carbonated subcontinental mantle. No consideration is given to the melting of carbonated eclogite or carbonate-bearing metasomatized lithospheric mantle. The volume of the magma formed is not specified and it is not explained how continued partial melting at a single site can lead to the formation and maintenance of a single mantle-to-crust conduit (see Fig. 6 of Vasyukova & Williams-Jones 2022), through which is transported the large volume of the magma required for the metasomatic genesis of vast amounts of mafic rocks in the upper crust. Why melting is restricted to small volumes and why melting is initiated or ceases is not considered. In addition, any discussion of the energetic constraints on carbonate-silicate interaction is neglected.

The magma volume problem is further exacerbated by the reactions with mantle conduits by wehrlitization processes which can result in conduit blocking and magma solidification in the mantle (see Schmidt *et al*. 2024; p. 14).

The parental and metasomatizing "carbonatite magmas" are considered NOT to contain significant silica, thus all Si, Al, Na, and K, *etc.* are derived from the country rocks. We consider this to be an unreasonable assumption for which there is much contrary evidence, as discussed above.

Metasomatic reactions are considered to be driven by "over-pressure fracture-induced loss of CO_2" (Vasyukova & Williams-Jones 2022; p. 3). This is an undefined and unexplained process which ignores enthalpy and free energy relations (see below).

The "carbonatite magma" is considered to have a very low viscosity as calculated, but not determined, by Genge *et al*. (1995). This is an unknown parameter especially because if the parental magma contains other components, such as silica, the viscosity would be increased and the magma percolation processes inhibited.

The relative volumes of country rocks and magma involved in metasomatic processes are not discussed. Vasyukova & Williams-Jones (2022) conceived the concept after observing, at the St Honoré complex, stockworks consisting of thin (<1 cm) zones of phlogopite adjacent to carbonatite veins emplaced in syenite. The formation of the phlogopite was ascribed to metasomatism when magnesiocarbonatite magma reacted with syenite and which led to the replacement of K-feldspar to form phlogopite plus calcite. Note that *all* of the magnesiocarbonatite is considered to be consumed in this reaction. From this observation, Vasyukova & Williams-Jones (2022) transformed this small-scale process to complexes in which the volume of the mafic rocks greatly exceeds the carbonatites present at the current level of exposure (*e.g.*, Salitre-I, Phalaborwa, Kovdor), and for which there is no evidence for a parental "magnesiocarbonatite magma". Apart from the inherent thermodynamic problems, to generate the substantial volume of all of these mafic rocks by metasomatism the process must require at least similar volumes of "magnesiocarbonatite magma" with concomitant formation of large volumes of calcite carbonatite residua. Significantly, the latter are not present in the expected amounts in any of the complexes discussed by Vasyukova & Williams-Jones (2022).

There are no explanations for the formation of the associated undersaturated silicate rocks which in many complexes are emplaced prior to the pyroxenites, *e.g.*, ijolite-urtites and melilitolites predate pyroxenites at Kovdor (Krasnova *et al.* 2004).

In support of their proposals, Vasyukova *et al*. (2022) presented a series of experiments in which $CaCO_3$, $MgCO_3$, and Na_2CO_3 were reacted with quartz at 900–1200 °C at 200 MPa to produce three "domains": Na(Ca)-rich glass; a zone of wollastonite, diopside, and forsterite; and one that was carbonate-rich. On this basis, they suggested that these reactions mimic the proposed antiskarn zonation observed in some carbonate-alkalic rock complexes (*e.g.*, Kovdor, Salitre-1). However, these experiments cannot represent the actual geological conditions present during the presumed formation of antiskarns, as the experimental reaction conditions are not adiabatic; that is, heat must be continually added to maintain a constant temperature or the reactions will terminate. Such conditions certainly cannot be met when the intruding magma is at a higher temperature than the country rock and heat must be transferred from a liquid to a solid to promote the reactions. We suggest below that the process must be considered in terms of constant enthalpy and not one of free energy minimalization as inferred by Anenburg & Walters (2024). It is not entirely clear whether Vasyukova & Williams-Jones (2022), Williams-Jones & Vasyukova (2023), and Vasyukova *et al*. (2022) envisage some assimilation of the host rock or only metasomatic transfer of components from the magma without assimilation. However, any form of assimilation will cause temperature decrease, viscosity increase, and crystallization of the current liquidus phase, *i.e*., calcite. Vasyukova & Williams-Jones (2022) use the term "metasomatic exchange", which implies a two-way transfer of material, and they also write "assimilation of Si (and Al) from the wall-rocks culminates in the magma having a Si (and Al) content sufficiently high to crystallize alkaline ultrabasic rocks".

Geological Evidence for and Against the Antiskarn Process

The antiskarn hypothesis assumes that all, or most of, the silicate rocks in alkaline complexes are metasomatic in origin and that the parental magma to all complexes is a "magnesio-carbonatitic magma". The hypothesis originally developed for Nolans Bore (Anenburg & Mavrogenes 2018) was extended by Vasyukova & Williams-Jones (2022) for some specific plutonic complexes which are considered to consist of substantial amounts of "pyroxenite" (*e.g.*, Salitre-I, Kovdor, Phalaborwa). The many other alkaline rock-carbonatite complexes containing ijolite-suite rocks but which do not contain substantial volumes of pyroxenite were ignored. Although Vasyukova & Williams-Jones (2022) never actually suggested that their hypothesis should be globally applicable, it has been uncritically adopted for a diverse variety of subvolcanic and plutonic alkaline rock-carbonatite complexes. It is evident that if the antiskarn hypothesis were to be a universal petrogenetic process, then pyroxenite margins to alkaline complexes should be the norm rather than the exception. However, this does not appear to be the actual situation, and some of the geological evidence relevant to the hypothesis is discussed below.

Salitre-I, Brazil

One of the key examples of the "carbonatite magma"-mediated metasomatic (or antiskarn) process cited by Vasyukova & Williams-Jones (2022) is the Salitre-I complex of the Brazilian Alto Paranaiba Province (APIP), for which it is claimed that clinopyroxenites form the bulk of the complex, regardless that these authors state that "the clinopyroxenites typically contain less than 50 modal % clinopyroxene" (see Figs. 4 and 5 of Vasyukova & Williams-Jones 2022). The sum of the other major constituents, phlogopite, apatite, perovskite, Ti-garnet, and magnetite, typically exceeds that of clinopyroxene and olivine. Barbosa *et al.* (2012) state that only one of 93 samples investigated by them has over 80 vol.% clinopyroxene and none exceed 90 vol.%. Clearly, these rocks, which are termed bebedourite by Brazilian petrologists (Barbosa *et al.* 2012), are not simple clinopyroxenites of the type proposed by Vasyukova & Williams-Jones (2022) in their metasomatic reactions. The simplified geological map of Salitre-I presented by Vasyukova & Williams-Jones (2022) glosses over the petrological complexity of the bebedourites as reported by Barbosa *et al*. (2012, 2020), who conclude on the basis of petrographic evidence that all of bebedourite suite rocks are cumulates and that the parental magmas have, as shown by mineral compositional evolution, undergone fractional crystallization. Significantly, Barbosa *et al.* (2012, 2020) do not report that any metasomatic features are present. Similar conclusions have been made for Tapira bededourites by Brod (1999) and for the Phalaborwa complex by Barbosa *et al.* (2012). Vasyukova & Williams-Jones (2022) do not discuss any of these data or why, as the Salitre-I complex is emplaced in metasedimentary rocks, how the significant enrichment in K, Ti, and P in the magmas which formed these rocks is achieved. In summary, there is no evidence for carbonatite magma-mediated metasomatism at Salitre-I, a conclusion which can be extended to other Brazilian APIP alkaline rock-carbonatite complexes: Serra Negra (Grasso 2010), Catalão-II (Palmieri *et al.* 2022), and Araxá (Biondi & Braga 2024).

Kovdor, Russia

Another key complex cited by Vasyukova & Williams-Jones (2022) and Vasyukova *et al.* (2023) as an example of carbonatite magma-mediated metasomatism is the Kovdor

complex (Russia). As with Salitre-I, a simplified geological map is presented which ignores the geological and petrographic complexity of the complex as described by Krasnova *et al.* (2004) and Rimskaya-Khorskova & Krasnova (2002). The only evidence cited for carbonatite-forming-magma-mediated metasomatism is that, in common with the Brazilian APIP complexes, the complex is zoned from a dunite core though clinopyroxenites to ijolite. However, the complex has been interpreted to have formed by fractional crystallization of a carbonated melanephelinite magma (Veksler *et al.* 1998) with the formation of *cumulate* dunites and pyroxenites. Gudelius *et al*. (2023) have suggested that there are two contrasting types of ultramafic rocks at Kovdor: some with cumulate textures containing olivine with high Ni contents and others which lack cumulate textures and consist of Ni-poor olivine, calcite, biotite, apatite, and baddeleyite. The latter are termed "metasomatic rocks" by Gudelius *et al.* (2023), even though there is no evidence presented for such an origin and regardless that they exhibit many complex igneous crystallization textures and that they form veins and segregations as illustrated by Rimskaya-Khorskova & Krasnova (2002). The "metasomatic ultramafic rocks" are essentially late-stage low temperature differentiates and are better termed phoscorites (Krasnova *et al*. 2004) rather than "ultramafic rocks". These rocks, on the basis of their mineralogy, also have affinities to aillikite-carbonatite magmatism. Appealing to the Ni content of olivine to distinguish these rocks from those with cumulate textures is unsupportable, as olivines crystallizing from Ni-poor late differentiates will by definition be Ni-poor. Many of these rocks can by interpreted in terms of experimental studies of the system $CaO–MgO–SiO_2–H_2O–CO_2$ (Franz & Wyllie 1966), which shows that liquidus olivine can crystallize with calcite at temperatures as low as 605 °C; metasomatism is thus not required.

Other serious problems with a metasomatic origin for all of the rocks forming the Kovdor complex are that there are no explanations given as to how a "magnesiocarbonatite magma" can by metasomatic reactions form the ijolites and melilitolites which constitute major parts of the complex. The ijolite ring dike was apparently one of the initial intrusions at Kovdor. Although this dike is in contact with the country rock Archean gneisses, there is no evidence for a metasomatic origin and no metasomatic pyroxenites have been formed at these contacts. In summary, we consider that all of the various rock types at Kovdor have been formed by differentiation, as suggested by Veksler *et al.* (1998).

Fengzhen, China

A particularly unfortunate invocation of the antiskarn hypothesis is the Fengzhen area, in which pyroxenites composed of Al-rich diopside and syenites are allegedly geographically associated with carbonatites as veins with tonalite-trondhjemite-granodiorite (TTG) and dioritic gneisses (Su *et al.* 2023). The syenites occur as xenoliths in the pyroxenite. Curiously, Su *et al.* (2023) do not describe the "carbonatites" or the relationships of the "carbonatite" to the silicate rocks in any detail apart from illustrations showing the presence of calcite crystals intergrown with diopside and hyalophane. Bulk compositional data or photomicrographs of carbonatite are not presented and all geochemical data were obtained from single calcite crystals in the silicate rocks. Note that Xu *et al.* (2019) illustrate "carbonatite" xenoliths in pyroxenite and granulite. Neither article ever shows that *mineralogically bona fide* carbonatites were ever present as discrete intrusions at Fengzhen. Su *et al.* (2023), following Vasyukova & Williams-Jones (2022), have simply assumed that "large volumes of carbonatites" have all been consumed by metasomatic reactions to form pyroxenites and syenites. On the basis of REE data Su *et al*. (2023) show that at least two varieties of calcite are present, with those in the syenite exhibiting negative Eu anomalies, in contrast to the absence of Eu anomalies for calcite in the pyroxenites. These data suggest that the calcite in the syenites formed after differentiation of the syenite-forming magma, the Eu anomaly reflecting prior feldspar crystallization. Coupled with the petrographic images presented by Su *et al*. (2023), we suggest that the calcites are merely late-stage hydrothermal minerals and that no *bona fide* "carbonatites" were ever present at Fengzhen. If the silicate rocks were formed by metasomatism, the "carbonatite" should be younger than these Paleoproterozoic silicate rocks. However, Su *et al.* (2023) do not give any radiometric age data for the calcite (or "carbonatites") to support their hypothesis. Note that Xu *et al*. (2019) consider the "carbonatites" to be contemporaneous with the silicate rocks. Su *et al.* (2023) also claim, on the basis of Ca/Pb-Sr bulk mixing models, that the proportions of country rock granite to carbonatite required to form the pyroxenites and syenites are 70–90% and 90–95%, respectively. Such extremely high mixing proportions are thermodynamically extremely unlikely due to thermal considerations (see below). Curiously, the syenite which is judged to form at the highest degree of assimilation occurs as xenoliths in the pyroxenite which allegedly formed with the least degree of assimilation. In summary, we suggest that Su *et al.* (2023) have simply failed to recognize that the pyroxenites and syenites are undoubtedly merely components of the regional gneiss complex. Su *et al.* (2023) make no comments regarding the conclusions of Xu *et al.* (2019) that the Fengzhen pyroxenites, syenites, and "carbonatites" were all formed during deep slab subduction at more than 1.9 Ga followed by slab break off at *ca*. 1.8 Ga. In this scenario, all of the rocks of the Fengzhen area are

formed from mantle-derived magmas and no antiskarn processes are involved.

Chinese Giant REE deposits

Although there is a consensus that Chinese Giant REE deposits (Ju *et al*. 2025), such as those of the Mianning-Dechang belt (Maoniuping, Lizhuang, Muluozhai, Dalucao), can be considered as plate-boundary carbonatites which are ultimately derived from enriched mantle sources (Liu *et al*. 2025, Chakhmouradian *et al*. 2025), there have been recent suggestions that antiskarn processes are partially involved in their genesis, such as the REE-enrichment of the Maoniuping deposit (Zheng *et al*. 2023, Liu & Anenburg 2025).

Although a detailed critique of Zheng *et al*. (2023) is beyond the scope of this work, it is evident that much of the genetic hypothesis for this deposit is not well-founded. Specifically, Zheng *et al*. (2023; p.29) suggest, but do not prove, that an initial "fertile carbonatite melt was derived from a carbonate-silicate magma by liquid immiscibility at shallow crustal levels". This initial melt is then suspended in the silicate melt, which prevents it from reacting with basement rocks. It eventually undergoes crystallization with the formation of calcite plus minor phlogopite and riebeckite, but remains Si-deficient. Increases in the concentration of alkalis and volatiles are considered to lower the viscosity of the carbonated melt, which then ascends faster than silicate melt. Further ascent leads to contamination by silicate rocks from antiskarn reactions at *ca*. 600 °C resulting in the formation in the "carbonatite melt" of liquidus phlogopite, sodic pyroxenes, and amphiboles, together with reactions involving Na_2CO_3, K_2CO_3, and $Ca(Mg,Fe)(CO_3)_2$. The silicate magma evolves separately and presumably forms the associated quartz syenites, although Zheng *et al.* (2023) avoid this detail. At Maoniuping, the volume of the ore bodies appears to be very large relative to the supposed associated quartz syenites, and on a volumetric basis it is impossible that these can be derived from the syenites. In addition, geological maps (Zheng *et al*. 2023, Liu *et al.* 2025, Chakhmouradian *et al.* 2025) show that the Mianning-Dechang REE-rich carbonatites form a regional dike swarm rather than having a constant relationship only to the quartz syenite, suggesting that they have independent sources. Apart from these geological constraints, we consider that the Zheng *et al.* (2023) genetic scheme is at the outset petrologically not sound, in particular because liquid immiscibility is invoked, disregarding all the evidence provided by Gittins & Mitchell (2023) against this process. Further, the origins of the initial carbonate-silicate magma are not discussed, and it is not explained how and why partial separation of the two liquids occurs. The antiskarn reactions involving alkali carbonates, Si, and Al from the country rocks are a particular problem, as the only "evidence" for the presence of the alkalis is their occurrence in fluid/melt inclusions and the supposed deficiency in Si and Al of the carbonatite-forming magma. The alkali-bearing inclusions are actually most probably residual fluids derived from the carbonatite-forming magmas rather than relicts of antiskarn reactions. No metasomatic pyroxenites are produced in the country rock granites or the quartz syenites by the carbonatite dikes. The Zheng *et al*. (2023) petrogenetic scheme is overly complex and can be completely avoided by considering the carbonatites and silicates to be formed from independent mantle-derived magmas created by direct partial melting of a plate-boundary carbonated eclogitic source.

In an extreme example in support of the antiskarn process, Liu & Anenburg (2025) have suggested that diopside and aegirine mantling quartz syenite xenoliths at Maoniuping result from reaction of carbonatite-forming magma with this syenite. The basis for this claim is that the carbonatite-forming magma is considered to be Si-free and that *all* Si for the formation of diopside mantles was supplied by the quartz syenite. In addition, Liu & Anenburg (2025, p. 4) state that, with respect to diopside, MgO is supplied from the "carbonatite melt". Unfortunately, given that dolomitic carbonatites are absent at Maoniuping (Liu & Anenburg 2025, p. 2), this contradiction to the proposed antiskarn process is not further explored, and the previous suggestion by Yin *et al*. (2021) that the pyroxenes have formed by reaction with a silica and Mg-bearing calcite carbonatite is simply ignored. Liu & Anenburg (2025, p. 4) also suggest that Na_2CO_3 is present in the melt and contributes to the formation of aegirine, regardless that there is no evidence for this component, that Na-REE-carbonates (carbocernaite, burbankite) are not present in the carbonatites, and that Na-poor bastnäsite is the only REE-bearing mineral.

The Creation or Consumption of Ultramafic Rocks

Some other authors, in contrast, consider carbonatite-forming magma as consuming rather than producing ultramafic rocks. For example, Pdah & Khonglah (2022) have described orbicules formed from pyroxenite xenoliths enclosed in calcite carbonatite in the Sung valley carbonatite complex of northeast India. They believe that the "metasomatic interaction" of the xenolith and "carbonatite melt" generated locally contaminated melt at the contact which then crystallized as forsterite-rich layers. Significantly, the pyroxenite is older than the carbonatite, as it is intruded by carbonatite. They invoke the term "antiskarn" for these orbicular layers around small xenoliths. They do not address the problem that incorporation of silica into the "carbonatite liquid" from xenoliths is of

very limited extent. It is difficult to reasonably extend the attendant assimilation process beyond the immediate vicinity of the xenoliths to involving a large body of carbonatite-forming magma. Exactly how much silica is incorporated into the carbonatite-forming magma is not estimated, but it presumably exceeds the <5 wt.% assumed by many carbonatite petrologists to be the limit of silica solubility.

Bouabdellah *et al*. (2022), in describing the Twihinate, Moroccan Sahara, carbonatite complex also refer to partially and completely resorbed mafic-to-felsic xenoliths of wall-rock sporadically dispersed throughout the carbonatite as further evidence of assimilation. They go somewhat further and invoke the antiskarn concept to explain "a succession of calc-silicate layers within the calcitic carbonatite". These consist of bands and lenses of diopside and of garnet which are believed to have "precipitated within the sövite intrusion itself close to the contact with the felsic country rocks". We are left with two contrasted functions allegedly attained by antiskarn activity, namely the creation and consumption of ultramafic rocks; they cannot both be right.

Giebel *et al.* (2019), in describing carbonatites in the Kaiserstuhl complex that contain disaggregated xenoliths of nosean syenite, believe that the carbonatite-forming magma has in the process increased its Si and Al levels to the extent where considerable amounts of mica crystallize. Note this is a subvolcanic complex and thus outside of the pressure-temperature regime initially proposed for antiskarn formation.

Walter *et al*. (2022) describe the essentially dolomitic Kieshöhe carbonatites of Namibia as being of two types: one containing abundant silicate rock xenoliths and the other with relatively few xenoliths. Silica is assumed to have been "mobilized in a fluid through post-magmatic xenolith resorption", but not to have had a major effect of producing calc-silicates in the carbonatite other than as biotite and pyroxene at the carbonatite/xenolith contacts. There is an indication of the importance they attach to silica enrichment by reaction of "carbonatite liquid" with siliceous host rocks in the statement "A useful indicator of contamination in carbonatites is the increased presence of silicates". Central to their thinking is, again, the notion that the silica content of carbonatite-forming magmas is insufficient to produce the amount of silicate minerals commonly present in carbonatites and must, therefore, have been enhanced by assimilation of siliceous host rock. Although the term antiskarn is not employed, it is evident from the references to the writings of Anenburg & Mavrogenes (2018) and Yaxley *et al.* (2022) that the concept is invoked.

For the Jacupiranga carbonatite in Brazil, Chmyz *et al.* (2022) describe the partial assimilation of clinopyroxenite xenoliths by "Mg-rich carbonatite magma" as having produced marginal zones of amphibole plus phlogopite, phlogopite, and olivine plus phlogopite. Unlike an earlier view that these are marginal metasomatic effects, they extend their interpretation to a carbonatite-forming magma having consumed diopside, becoming more calcitic in the process, and subsequently crystallizing the silicate minerals, saying "…antiskarns may be a suitable term to the Jacupiranga reaction rocks". Again, however, it seems questionable to extend to a large body of magma the production of a layer of contaminated magma adjacent to xenoliths, and the authors do speak of the limited extent in stating "assimilation of clinopyroxenite accounts for local increases in silica activity of carbonatite magma…". Note that at Jacupiranga the volume of olivinites and pyroxenites far exceeds the volume of carbonatite, and it is not plausible that the rocks have all been formed by antiskarn reactions.

Yaxley *et al.* (2022) deal with the concept on a larger scale, but even here it is not clear whether the antiskarn is a marginal silicate-rich rock or whether the assimilation of silica from the country rock penetrates deep into the carbonatite-forming magma to explain the presence of silicates in excess of what can be explained by the limited amount of silica (<5 wt.%) assumed by many petrologists to be present in mantle-derived carbonatite-forming magma. They seem to hedge their bets by calling antiskarn "A zone within a carbonatite intrusion".

Alkaline Rock-Carbonatite Complexes; Lacking Ultramafic Rocks (Failed Antiskarns?)

Proponents of the antiskarn hypothesis invariably do not refer to the many alkaline rock complexes lacking ultramafic rocks and which show no evidence for reaction of carbonatite with country rocks. Although there are far too many of these occurrences to discuss here, we consider below some examples of carbonatites of diverse age and geological setting intruded into Si-rich country rocks which should have provided the maximum opportunity for antiskarn reactions, if these are to be considered as a viable process.

Marinkas Quellen, Namibia

The Marinkas Quellen complex (Smithies & Marsh 1998) consists of a southern intrusion of magnetite-bearing dolomite carbonatite and a partial ring of calcite carbonatite (Fig. 2). The northern intrusion consists of nepheline syenite intruded by an aegirine ferro-richterite calcite carbonatite with an eastern margin of dolomite carbonatite. Minor ferroan dolomite carbonatite intrudes this and the nepheline syenite. Pervasive sodic fenitization of the gneissic country rocks forms a 300 m wide zone around the complex. Pyroxenites, olivinites, and glimmerites are notably

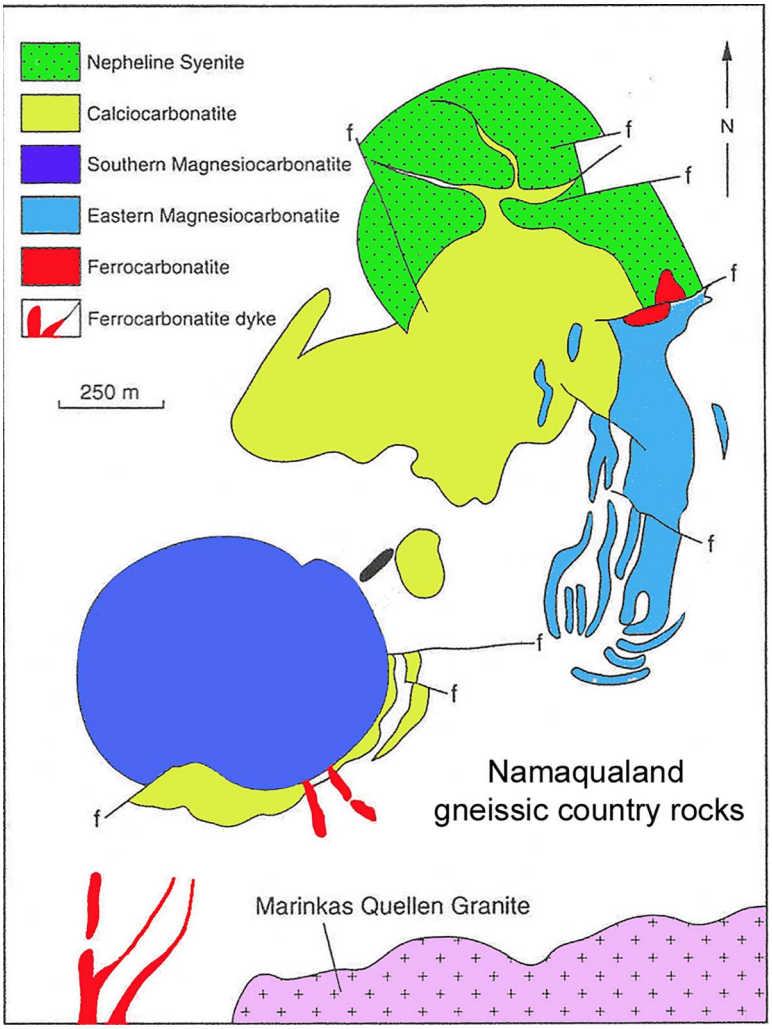

FIG. 2. Geological map of the Marinkas Quellen carbonatite complex (Namibia) after Smithies & Marsh (1998). Note that pyroxenites are not formed adjacent to the dolomitic carbonatites, in contradiction to the antiskarn hypothesis.

absent throughout or adjacent to the complex and are especially lacking around the southern magnesiocarbonatite, which should have been a prime location for any antiskarn reactions.

Safartôq and Qaqarssuk, Greenland

The 600 Ma Safartôq complex (Secher & Larsen 1980) consists of an outer ring of calcite carbonatite and an inner core of dolomite carbonatite with lenses of calcite carbonatite. The carbonatites are intruded into Proterozoic granodioritic and enderbitic gneisses which are transformed into a narrow zone (<50 m) of sodic fenites followed by a wide area of hematitized gneiss. The *ca.* 170 Ma Qaqarssuk complex (Knudsen 1985) consists of several ring dikes or sheets of calcite carbonatite enclosing and surrounded by granitic gneiss (Fig. 2). Minor late-stage dikes of dolomite and ferroan dolomite carbonatite are present. The gneisses are extensively fenitized with albite, aegirine, and alkali amphiboles replacing quartz. A minor occurrence of mafic fenite xenoliths in the carbonatite have mica-rich rims and are termed "ultramafic rocks" by Knudsen (1985). These are only present in one area of the complex where the fenite protolith was already rich in mafic minerals. The common feature of both complexes is that the pyroxenites and olivinites predicted by the antiskarn hypothesis are absent.

Siriwasan-Dugdha, India

These areas are characterized by intrusion of "carbonatite" into sandstones of the Bagh Group of sedimentary rocks. (Patidar & Agrawal 2022, Gwalani *et al*. 1990). These intrusions of calcite carbonatite into sandstones should be an ideal site for antiskarn reactions and where the formation of wollastonite antiskarns should be expected. However, the carbonates have merely infiltrated the sandstone and formed a calcite matrix to quartz grains which lack reaction mantles.

Thermodynamic Evidence for the Failure of the Antiskarn Process

Anenburg & Walters (2024) hypothesize that silicocarbonatites form by "leaching of SiO_2 from siliceous wall-rock by carbonatitic melts followed by reactions with the carbonatitic melt to form silicate minerals". The hypothesized petrogenesis of antiskarn rocks can therefore be treated as an assimilative process whereby two endmember bulk compositions, for example, a silicate-rich granitic (*sensu lato*) wall-rock and a "carbonatitic magma", react and thermally equilibrate to form an assemblage that approximates thermal and chemical equilibrium. The assimilation process is unlike typical scenarios applicable to regional metamorphism or closed system igneous rocks. In the latter, the thermodynamic problem is as follows: given a fixed bulk composition and under the *imposed* constraints of constant temperature ($T = T_{surr}$) and fixed external pressure ($p = p_{ext}$), what is the equilibrium phase assemblage? The equilibrium state can be found by minimization of the Gibbs energy (Ghiorso & Kelemen, 1987) at the *externally prescribed* p_{ext} and T_{surr}. The key concept in Gibbs energy minimization is that the system is surrounded by a diathermal (perfectly conducting) flexible boundary such that the system temperature and pressure is maintained equal to that of its surroundings throughout the equilibration process. Anenburg & Walters (2024) follow that prescription. That is, the calculation of the phase assemblage at some pressure and temperature for a specified bulk composition is found by minimization of the Gibbs energy at the conditions of temperature and pressure specified *a priori*. In this conceptualization, the system (magma plus host) is immersed in a thermal bath and is surrounded by a diabatic (perfectly heat conducting) and flexible (to allow for volume change) boundary such that the contents of the system remain at the externally imposed p_{ext} and T_{surr}.

In contrast, the antiskarn assimilative process involves the reactive interaction of hot carbonatite-forming magma (melt, mush, or mostly solid, hereafter collectively referred to for brevity as carbonatitic magma) with colder silicate-dominated wall-rock (hereafter referred to as granite for brevity). This interaction is approximated as an isenthalpic process such that the total enthalpy of the equilibrated mixture in the final state equals the sum of the enthalpies of each endmember in their initial states, each at a unique initial temperature. In this scenario, with constraints of constant enthalpy and pressure, the appropriate thermodynamic extremal criterion for equilibrium is the maximization of the combined system entropy. Other constraints, such as volatile fugacities, could also be externally imposed. In thermodynamic software packages such as EC-RAFC (Spera & Bohrson 2001, 2002, 2004, Bohrson & Spera 2007), MELTS (Ghiorso & Sack 1995, Gualda *et al.* 2012), or MCS (Bohrson *et al*. 2014, Bohrson *et al*. 2020, Heinonen *et al.* 2020) assimilation is treated as an isenthalpic process in accord with the pioneering study of Taylor (1980) who first quantified the heat balance between cooling and crystallization of magma and heating and partial, or wholesale, melting of host rocks based on the deductions of Bowen some 50 years earlier (1928, chapter 10). In an isobaric-isenthalpic process, the enthalpy of the final state is identical to the sum of the enthalpies of the endmembers in their initial (pre-reaction) state, each at a unique temperature. In the case of the antiskarn scenario, interaction between the reactive endmembers of magma and country rock initially at different temperatures (T_{oc} and T_{og}, for carbonatitic magma and granitic wall-rock, respectively) takes place such that the total enthalpy is constant. Given the isenthalpic constraint, the temperature of the final system is determined as part of the calculation rather than being imposed *a priori* as in Gibbs energy minimization. The isenthalpic processes is considered a better approximation to the geologic process when magma interacts with wall-rocks. In physical terms, the question is, when emplaced into colder wall-rock, is there sufficient latent and sensible heat in the carbonatitic magma to (1) heat wall-rock and (2) provide the energy requirements for the endothermic reactions that convert carbonates to silicates? This is the question pursued here using two simple thermal/reaction models. The first simple thermal model neglects the effects of endothermic reactions and hence provides a lower limit on the mass ratio of carbonatitic magma to wall-rock assimilant mass in order to reach a given final temperature. In the second isenthalpic model, the effects of endothermic reactions are included. Inclusion of carbonate-silicate reactions, which require that energy be provided by the carbonatitic endmember, limits the extent of the silicate-forming reaction process rather profoundly.

TABLE 1. THERMODYNAMIC DATA FOR THE REACTION OF $CaCO_3$ WITH SiO_2

Temperature, pressure	$\Delta G_{p,T}$ (kJ/mol) $\Delta H_{p,T}$ (kJ/mol)	$\Delta G_{p,T}$ (kJ/kg Cc) $\Delta H_{p,T}$ (kJ/kg Cc)
25 °C, 100 kPa	+40.85	+405
	+89.34	+886
927 °C, 100 kPa	−96.79	−960
	+75.82	+752
927 °C, 100 MPa	−25.61	−254
	+76.30	+757

$CaCO_3$ (cc) + SiO_2 (qtz) ⇌ $CaSiO_3$ (wo) + CO_2 (fluid) with all crystalline phases at unit activity and CO_2 fugacity for pure component at temperature and pressure of reaction for CO_2 treated as a real gas.

Role of endothermic reactions

In Table 1 the Gibbs energy and enthalpy of the archetypical reaction

$$CaCO_{3\,(cc)} + SiO_{2\,(qtz)} = CaSiO_{3\,(wo)} + CO_{2\,(g)}$$

at several temperatures and pressures is recorded. Data for additional reactions are presented in the supplementary file (Tables A3 and A4), but this prototypical reaction suffices here. Perusal of Table 1 values shows a number of features: (1) at low T and 1 bar the reaction does not proceed to the right: the assemblage calcite plus quartz is stable; (2) at 1 bar and a magmatic temperature of 927 °C the reaction has a negative Gibbs energy and runs spontaneously *when placed in a thermal bath that can supply the heat of reaction of 752 kJ/kg of consumed calcite from the external environment*. Note that as pressure increases, the driving force of the reaction decreases, although it remains spontaneous and the thermal requirement increases but only slightly. This is mainly due to the change in the molar entropy of CO_2 gas with pressure. Above all, the salient point from Table 1 is the strongly endothermic quality of the reaction of carbonate with silicate to form pyroxene. The endothermic quality of the carbonate-silicate reaction holds for other carbonate-silicate reactions (see Supplementary file Tables A3 and A4) and implies large carbonatite to wall-rock mass ratios, which is generally inconsistent with field observations and the antiskarn hypothesis.

In the following sections, results from two isenthalpic assimilation models are presented. The first is a thermal model that ignores reactions. *Since the essential reactions are all endothermic, this model sets an upper limit on the efficacy of assimilation*. The second model incorporates the effects of endothermic reactions in which magmatic carbonate reacts with crustal silicates to generate silicate phases (generally pyroxenes and alkali amphiboles). The model derivations are provided in the supplementary file. Here we give a brief discussion of the conceptual basis, present some graphical results, and discuss the implications relevant to the antiskarn hypothesis. All quantities and symbols are defined in Table 2.

TABLE 2. NOMENCLATURE AND NUMERICAL VALUES

Symbol	Definition	Units	Properties set 1	Properties set 2	Properties set 3
h_g	enthalpy of granite	J		varies	
h_c	enthalpy of carbonatite	J		varies	
m_g	mass of granite endmember	kg		variable	
m_c	mass of carbonatitic endmember	kg		variable	
$\Re$	mass ratio m_c/m_g			variable	
C_{sg}	isobaric specific heat capacity of crystalline granite	J/kg·K	900	900	1100
C_{sc}	isobaric specific heat capacity of crystalline carbonatite	J/kg·K	1275	1200	1200
$C_{\ell g}$	isobaric specific heat capacity of granitic melt	J/kg·K	1375	1375	1300
$C_{\ell c}$	isobaric specific heat capacity of carbonatitic melt	J/kg·K	1400	1400	1300
T_{Sg}	granite solidus temperature	°C	600	600	650
T_{Sc}	carbonatite solidus temperature	°C	700	750	700
T_{Lg}	granite liquidus temperature	°C	1050	1000	1070
T_{Lc}	carbonatite liquidus temperature	°C	1100	1050	1100
Δh_{fg}	fusion enthalpy of granite	kJ/kg	280	280	250
Δh_{fc}	fusion enthalpy of carbonatite	kJ/kg	230	230	300
T_{og}	initial temperature of granite	K	300	300	300
T_{oc}	initial temperature of carbonatite	K	1150	1100	1100
T_f	post assimilation (final) temperature of mixture	K		computed at given $\Re$	

Model 1: Isenthalpic assimilation without reaction

Consider the thermal outcome of isenthalpic mixing of carbonatitic melt of mass m_c at initial temperature T_{oc} with granitic wall-rock of mass m_g at initial temperature T_{og}. Five thermal properties are assigned to each endmember: heat capacity in solid and liquid states, enthalpy of fusion, and solidus and liquidus temperatures. The thermodynamic question posed is, given an initial state and set of thermodynamic properties, what is the final temperature after isenthalpic equilibration as a function of the mixing (mass) ratio defined here by $\Re = m_c/m_g$? Once the initial conditions and properties are fixed, the solution yields an expression that gives a unique equilibrium temperature for a given mixing ratio $\Re$. For reference, the mass fractions of the endmembers are related to $\Re$ according to $f_g = (1 + \Re)^{-1}$ and $f_c = \Re(1 + \Re)^{-1}$ where f_g and f_c are the mass fractions of granite and carbonatite making up the mixture.

The computational strategy is to recognize that the final temperature (T_f) must lie between T_{og}, the initial temperature of wall-rock, and T_{oc}, the initial temperature of carbonatitic magma. Precisely where in that interval depends on the mixing ratio for a given set of thermodynamic properties. Clearly, as $\Re \to \infty$, $T_f \to T_{oc}$ whereas as $\Re \to 0$, $T_f \to T_{og}$. The calculation allows one to determine T_f for an arbitrary value of $\Re$ or *vice versa*. The important temperature intervals are depicted in Figure 3 along the temperature line defined by the extremal values of the endmembers in their initial states. The relative placement of the solidii and liquidii of the endmembers along this line can change depending upon bulk compositions, volatiles, pressure, and redox conditions; four representative examples of these placements are portrayed in Figure 3. The results presented here always specify which of the four possibilities (Fig. 3, a, b, c, or d) is used to generate a particular diagram. Although the numerical values of the required temperatures are not fixed, the order determines the appropriate temperature intervals and hence the enthalpy expressions required in the energy balance (see Appendix). The six temperatures of the model are defined in Table 1 and include the initial temperatures of wall-rock and magma, as well as their solidii and liquidii. If the order is changed, then the enthalpy balance equalities for each temperature interval are different. Table A1 (a–d) gives enthalpy balance equations appropriate for each temperature line. There is no significance to the relative location of the temperatures in the figure except the order.

Figure 3 reveals that there are five coterminous temperature intervals for T_f depending on the specific enthalpy h(T) relation for each endmember applicable in each prescribed temperature interval. Enthalpy expressions are given in the Appendix for the distinct relative temperature lines of Figure 3. As an example, for T_f in the subsolidus range $T_{og} \le T \le T_{Sg}$, Equations A1 and A7 are equated to express the isenthalpic condition to give the unique relationship between the mass ratio of carbonatitic magma to granitic wall-rock, $\Re$, and the temperature of the thermally equilibrated mixture, T_f, for the relative temperature distribution of solidii and liquidii of Figure 3a. The result is

$$\Re = \frac{C_{sg}(T_{og} - T)}{C_{Sc}(T_{Sc} - T_{Lc}) - \Delta h_{fc} + C_{lc}(T_{Lc} - T_{oc}) + C_{sc}(T_f - T_{Sc})} \quad (1)$$

The bounding temperatures of the limits can be used to determine the bounding values for $\Re$. At $T = T_{og}$, $\Re_{min} = 0$ since no mixing takes place and hence the final temperature is simply the initial wall-rock temperature. At the upper bound, the wall-rock solidus temperature for this interval, $T = T_{Sg}$, gives $\Re = \Re_{max} = 0.288$ using the parameters in Table 1. Since $f_c = \Re/(1 + \Re)$, $\Re_{max}$ determines the required fraction of carbonatitic magma in the mixture such that the final temperature falls at the wall-rock solidus, T_{Sg}. In this case, $f_{c\ max} = 0.224$. That is, for mass fractions of carbonatite in the mixture between zero and 0.224, T_f lies between the wall-rock temperature and T_{Sg} the wall-rock solidus of 600 °C from Table 1. Stated differently, if the fraction of carbonatitic magma in the mixture is less than about 22% by mass, the final temperature after isenthalpic mixing will not exceed the wall-rock solidus. The system is 'choked' by the cold wall-rock, and the end product is crystallized carbonatitic magma and subsolidus granite; there is not sufficient enthalpy in the combined endmembers to give a final temperature that exceeds the granite solidus in this case.

The curves in Figure 4 have been constructed using the method outlined above (full derivation in the Appendix) based on the relative location of solidii and liquidii depicted in Figure 3. Properties for the three cases illustrated are collected in Table 2. In Figure 4, the equilibrated temperature of the initially polythermal wall-rock-carbonatite system is depicted as a function of the fraction of carbonatitic magma, f_c, making up the mixture. Three different property sets are depicted that show relatively small differences in the relationship between the fraction of carbonatite in the final state and equilibrated temperature. To raise wall-rock to its solidus at ~600 °C requires about 20% of carbonatitic magma to cool and crystallize with little dependence on specific property values. To approach the granite liquidus at 1050–1100 °C requires ~90% carbonatitic magma involvement. These results show the need for large fractions of carbonatitic involvement during isenthalpic mixing and antiskarn formation. Field observations do not support such large fractions of the carbonatitic endmember in putative antiskarn rocks.

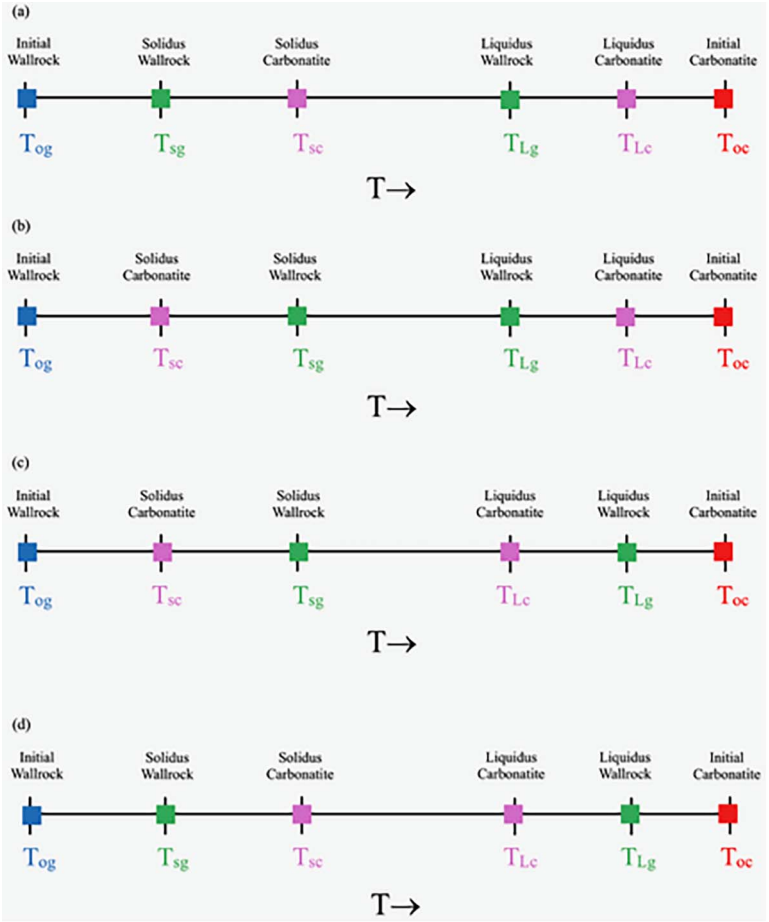

FIG. 3. The thermal models discussed in the text and derived in Appendix 1 are based on a specific arrangement of solidii and liquidii for the assimilation endmembers. Numerical results presented in this study focus on the temperature line depicted in 3a; the other possibilities (b, c, and d) are portrayed for completeness. For each of the four possible temperature lines, the applicable enthalpy balance expressions are given in Tables A1a–A1d in the supplementary file. The temperatures T_{og}, T_{Sg}, T_{Lg}, T_{Sc}, T_{Lc}, and T_{oc} refer to the initial temperature of wall-rock, solidus of wall-rock, liquidus of wall-rock, solidus of carbonatite, liquidus of carbonatite, and initial temperature of carbonatitic magma, respectively.

Reactions are not accounted for in this simple thermal model. Since the relevant reactions are quite endothermic, the results of the simple thermal model are a limiting case. When reactions are considered (see below) the mass of carbonatitic magma required to achieve a specific temperature is larger, sometimes considerably so, and thus does not support the antiskarn hypothesis based on energetic grounds.

Model 2: Isenthalpic assimilation with reaction

The simple thermal model presented above is modified here to incorporate carbonate-silicate reactions. There are many potential reactions to consider. Comprehensively accounting for all possibilities requires implementation of multicomponent-multiphase thermodynamic models such as MELTS (Ghiorso & Gualda 2015), THERMOCALC (Powell & Holland 1988, Holland & Powell 2011), Perple_X (Connolly 1995), Theriak-Domino (de Capitani & Petrakakis 2010), or MAGEMin (Riel *et al.* 2022). Unfortunately, none of these codes can consider phase relations for isenthalpic processes across the range of compositions required. Here, it is sufficient to consider representative reactions between carbonate and silicate phases. A number of such reactions are given in the Appendix. The common feature is that carbonatitic magma (written in terms of a single component) reacts with wall-rock silicates to form other silicates and liberate

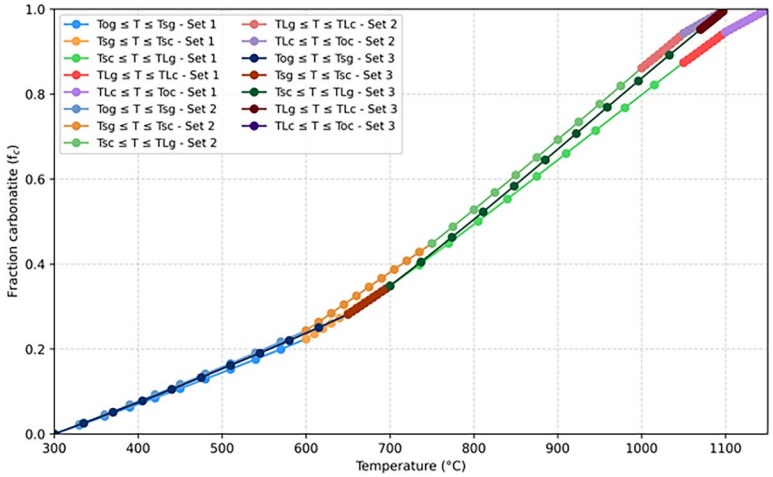

FIG. 4. Relationship between the final (equilibrated) temperature and the mass fraction of carbonatite endmember for isenthalpic equilibration between a carbonatitic magma, initially at temperature T_{oc} and granitic wall-rock at initial temperature T_{og}. The parameters used in each model are given in Table 2 (sets 1–3). In all cases the temperature line of Figure 3a is implemented with the initial temperature of the wall-rock equal to 300 °C. Solidii and liquidii vary, as do fusion enthalpies and isobaric specific heats, across the three parameter sets. The similarity of f_c–T trajectories indicates that results are robust to changes in detailed assumptions about properties and initial conditions. For post assimilation temperatures to attain the solidus of granitic wall-rock requires more than ~30% by mass of carbonatitic magma. These results neglect the effects of endothermic reactions between carbonate and silicate and hence represent a minimal carbonatite magma fraction to attain any given equilibrated (final) temperature.

CO_2. Values of the enthalpy, entropy, isobaric heat capacity, and volume change for a number of reactions are given in Table A3. At crustal pressures and magmatic temperatures these reactions possess negative Gibbs energies. Significantly, all reactions are endothermic roughly equaling $\sim 10^5$ J per mole of carbonate consumed. The volume change of the solids for all reactions is negative, which increases the spontaneity of the reaction as pressure increases, although the effect is relatively small.

Values in Table A3 have been used to compute the Gibbs energies and enthalpies of reactions listed in the supplementary file at typical crustal temperature-pressure conditions in Table A4. The reactions are spontaneous and endothermic at magmatic temperatures and upper crustal depth. Heat is consumed in these decarbonation reactions, and this puts an additional thermal burden on the high-temperature thermal reservoir (the carbonatitic magma) that must supply heat to relatively cold wall-rock undergoing reaction. Evaluation of the reaction enthalpies for typical reactions at appropriate conditions (700–1100 °C) reveals values around +1000 kJ per kg of carbonate reactant (Table A5). These values are generally *larger* than typical fusion enthalpies for silicates. One anticipates, consequently, that the limits of the thermal model previously presented move in a direction to make reaction of carbonate with wall-rock silicates *less* likely in the sense that the ratio $\Re = m_c/m_g$ will be higher to achieve any given thermally equilibrated temperature under the isenthalpic constraint.

Also collected in Table A3 are the critical mass ratios of carbonate and silicate phase reactants. These ratios are defined by reaction stoichiometry. When the reactants are in the critical mass ratio denoted $\Re_c^*$ for a particular reaction neither carbonate nor silicate reactant is limiting and the heat absorbed to convert reactants to products is at a maximum: there is exactly sufficient reactant to completely convert into reaction products. The mass fraction of carbonate reactant in the mixture that provides the maximum absorbed enthalpy is denoted f_c* and is provided in Table A3. The maximum heat consumption takes place when the carbonate to silicate ratio is in the optimal proportion defined by the reaction stoichiometry. For example, adopting Reaction 1 for illustration, the maximum consumption of enthalpy occurs when the fraction of carbonate in the reactant mixture or, as an alternative description, the mass ratio are, respectively,

$$f_c^* = M_{cc}\nu_{cc}/(M_{cc}\nu_{cc} + M_{qtz}\nu_{qtz})$$

or

$$\Re_c^* = M_{cc}\nu_{cc}/(M_{qtz}\nu_{qtz}) \qquad (2)$$

where M is the molar mass of the subscripted phase (*i.e.*, for reaction j = 1, calcite or quartz in this example)

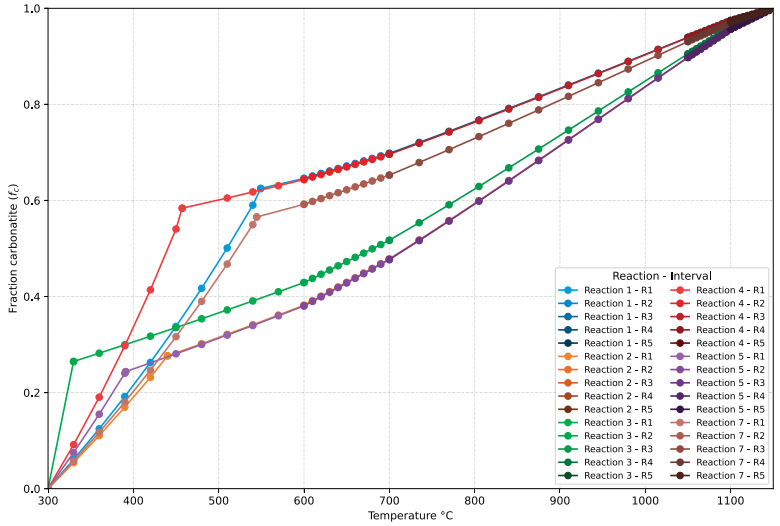

FIG. 5. Relationship between the final (equilibrated) temperature and the mass fraction of carbonatite endmember for isenthalpic equilibration between a carbonatitic magma, initially at temperature T_{oc}, and granitic wall-rock at initial temperature T_{og}, that includes the effects of endothermic reactions 1–7 given in Appendix 1. In Table A3 (supplementary file) the critical mass fraction of carbonatite in the mixture is given for each reaction. Parameter set 1, given in Table 2, applies to all curves. The segmented nature of the curves arises because the limiting reactant, either silicate or carbonate, changes as the mass fraction of carbonatitic endmember of the assimilation process increases. In all cases the temperature line of Figure 3a is implemented with initial wall-rock temperature of 300 °C. For post assimilation temperatures to reach the wall-rock solidus requires 40 to 65% by mass of carbonatitic magma. Reactions between Ca and Mg carbonate with plagioclase and quartz in wall-rock impose an especially large thermal penalty *via* endothermic reactions. Such large carbonatite fractions are not consistent with field observations.

and ν represents the stoichiometric coefficients of the respective reactants. For this particular reaction (j = 1), $f_c^* = 0.625$ or, cast as a ratio, $\Re^* = \frac{m_c^*}{m_g} = 1.67$ (Table A3). When calcite and quartz are in mass ratio 1.67, the enthalpy requirement for consumption of all reactants is maximal on a per kilogram basis. When $CaCO_3$ is the limiting reactant $\Re < \Re^*$ there is insufficient carbonate to react with excess quartz and when $\Re > \Re^*$ quartz is the limiting reactant (excess carbonate). Each reaction defines a unique and optimal $\Re_j^*$ where the subscript j is the index to a particular reaction enumerated in the Supplementary file. The enthalpy requirement depends on which reactant is limiting and can be written for any reaction:

$$\Delta h_{rxn} = \Delta h_{jc}{}^* m_c \text{ for } \Re < \Re^* \quad (3)$$

or

$$\Delta h_{rxn} = \Delta h_{jc}{}^* \frac{\Re^*}{\Re} m_c \text{ for } \Re > \Re^* \quad (4)$$

In Equations 3 and 4, $\Delta h_{jc}{}^*$ represents the enthalpy of the j^{th} reaction per kg of carbonate reactant. The key aspect is that at fixed pressure reaction of carbonate with silicate consumes enthalpy that is at a maximum when the mass ratio of reactant carbonate to reactant silicate equals the critical ratio defined by the reaction stoichiometry.

In order to incorporate the effects of endothermic reactions on the thermal state of carbonatite-wall-rock mixtures, the enthalpy balance equations were modified to include reaction enthalpies. The value of $\Re^*$ depends on the specific reaction and is indexed according to $\Re_j{}^*$ where the index j refers to the reaction number and the asterisk reminds one that this mass ratio is the one defined uniquely for each reaction by its stoichiometry. The temperature intervals used here are identical to those used in the thermal model (Fig. 1). The expressions for enthalpy, h(T), for the endmembers are presented in the supplementary file. These expressions are valid in each temperature range as defined in the simple thermal model. The effects of reaction enthalpy are included with the 'granite' endmember since the endothermic reactions are a heat sink with the required energy being supplied by the initially hotter carbonatitic magma. There are now two expressions for the enthalpy of wall-rock: one for $\Re < \Re^*$ and one for $\Re > \Re^*$. The expressions are equations A14–A17 given in the electronic appendix as supplementary material.

In Figures 5 and 6 results are portrayed for 11 of the reactions listed in the supplementary file, identified

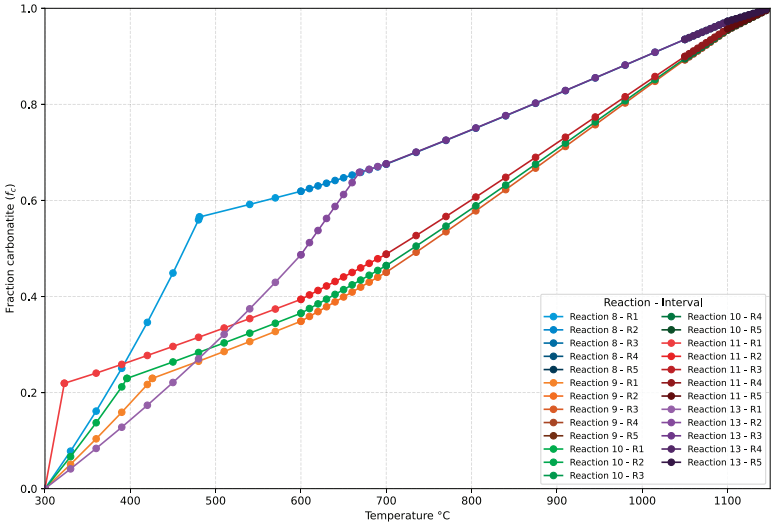

FIG. 6. Relationship between the final (equilibrated) temperature and the mass fraction of carbonatite endmember for isenthalpic equilibration between a carbonatitic magma, initially at temperature T_{oc}, and granitic wall-rock at initial temperature T_{og}, including the effects of endothermic reactions 8, 9, 10, 11, and 13 listed in the supplementary files. The segmented nature of the curves arises because the limiting reactant, either silicate or carbonate, changes as the mass fraction of carbonatitic endmember increases. In Table A3 (supplementary files) the critical mass fraction of carbonatite in the mixture is given for reactions 8–13. Parameter set 1 (see Table 2) and the temperature line in Figure 3a are implemented with an initial wall-rock temperature of 300 °C. For post assimilation to attain the solidus requires ~40 to 60% by mass of carbonatitic magma. Reactions between dolomitic and sideritic carbonate with plagioclase and quartz in wall-rock impose an especially large thermal penalty *via* endothermic reactions.

by reaction number. The steep character of these curves at subsolidus wall-rock temperatures emphasizes the thermal penalty incurred when endothermic reactions are taken into account. Comparison of Figure 4 with Figure 5 shows the effects of including carbonate-silicate reactions on the relationship between temperature and fraction of carbonatite required in the mixture to attain that temperature. For Reaction 8, for example, the mass fraction of carbonatite in the mixture to reach the wall-rock solidus temperature increases by a factor of three compared to the thermal model without reactions (Fig. 4). With reactions accounted for, reaching the wall-rock solidus requires carbonatite mass fractions in the mixture of 0.4 to 0.6. To attain higher temperatures requires an even greater carbonatitic mass contribution. These large fractions of carbonatitic magma are not supported by field relations concerning relative volumes in the examples cited earlier.

In summary, the energetics of isenthalpic reaction and thermal equilibration of granitic wall-rock when assimilated by carbonatitic magma is modeled by consideration of the relationship between temperature of the post-mixing assemblage and the mass fraction of carbonatitic magma constituting the mixture subject to the isenthalpic constraint. This constraint explicitly allows for unique endmember initial temperatures, a natural condition of the assimilation process. Especially relevant to the antiskarn hypothesis is consideration of the effects of endothermic reactions. These place a significant thermal burden on the high-temperature (compared to wall-rock) carbonatitic endmember. Two models have been explored here. The first focuses on the thermal equilibration of initially cold wall-rock and hot carbonate-rich magma and finds a relationship between the endmember mass ratio and temperature upon thermal equilibration using endmember thermodynamic properties and initial conditions. Because it neglects endothermic reactions this model gives the *minimal* ratio of carbonatitic magma to wall-rock mass to attain a given equilibrium temperature. It shows that for final temperatures to exceed the carbonatite solidus, carbonatite mass fractions must exceed about 40% by mass in the mixture. A second model, incorporating the effects of endothermic reactions, reveals the penalty engendered by the inclusion of reactions: carbonatitic fractions rise even higher, up to ~60%. Such large carbonatitic fractions do not accord with any of the field observations reviewed earlier.

CONCLUSIONS

The objective of this contribution is to provide arguments against the antiskarn hypothesis. It is not to

discuss any of the other hypotheses currently proposed to explain the genesis of carbonatites and alkaline rock complexes. The discussion is relevant only to plutonic rocks, as the antiskarn hypothesis cannot be applied to volcanic provinces containing carbonatites.

We conclude on the basis of the above discussion that:

(1) There is no geological evidence to support the hypothesis that antiskarn processes are required to form ultramafic and/or silica undersaturated rocks in alkaline rock carbonatite complexes.
(2) Carbonatite-forming magmas are not deficient in silica and typically crystallize abundant primary silicate minerals.
(3) Antiskarn reactions are not supported by realistic isenthalpic thermodynamic models.
(4) Fluids derived from carbonatite-forming magmas can react with country rocks to form exoskarns (fenites) and minor ultramafic selvages around veins, but these reactions cannot result in the formation of the voluminous silicate rocks present in alkaline rock-carbonatite complexes.

Acknowledgments

Mitchell acknowledges the support of Lakehead University and Almaz Petrology. Gittins recognizes the support of the Natural Sciences and Engineering Council of Canada and the University of Toronto. Spera acknowledges support from the National Science Foundation, most recently NSF-2151039, and the University of California Santa Barbara and Bailey Estes (Colorado School of Mines) for assistance with calculations and figures. Ilya Veksler and Alexi Rukhlov are thanked for reviews of this work. Valerie Dennison is thanked for initial copyediting and Steve Prevec and Mackenzie Parker are thanked for editorial handling.

AI Statement: AI was not used in the preparation or writing of any part of this document.

References

Anenburg, M. & Guzmics, T. (2023) Silica is unlikely to be soluble in upper crustal carbonatite melts. *Nature Communications* **14**(1), 942. DOI: https://doi.org/10.1038/41467-023-35840-6

Anenburg, M. & Mavrogenes, J.A. (2018) Carbonatitic versus hydrothermal origin for fluorapatite REE-Th deposits: Experimental study of REE transport and crustal "antiskarn" metasomatism. *American Journal of Science* **318**, 335–366.

Anenburg, M. & Walters, J.B. (2024) Metasomatic ijolite, glimmerite, silicocarbonatite and antiskarn formation: Carbonatite and silicate phase equilibria in the system Na_2O–CaO–K_2O–FeO–MgO–Al_2O_3–SiO_2–H_2O–O_2–CO_2. *Contributions to Mineralogy and Petrology* **179**, 40. DOI: https://doi.org/10.1007/s00410-024-02109-0

Anenburg, M., Mavrogenes, J.A., & Bennett, V.C. (2020) The fluorapatite P-REE-Th vein deposit at Nolans Bore: Genesis by carbonatite metasomatism. *Journal of Petrology* **61**(1), egaa003. DOI: https://doi.org/10.1093/petrology/egaa003

Barbosa, E.S.R., Brod, J.A., Brod, T.C., Dantas, E.L., Cordeiro, P.F.O., & Gomide, S. (2012) Bebedourite from its type area (Salitre I complex): A key petrogenetic series in the Late-Cretaceous Alto Paranaíba kamafugite-carbonatite-phoscorite association. *Lithos* (2012), 144–145, 56–72. DOI: https://doi.org/10.1016/j.lithos.201204.013

Barbosa, E.S.R., Brod, J.A., Cordeiro, P.F.O., Brod, T.C., Santos, R.V., & Dantas, E.L. (2020) Phoscorites of the Salitre I complex: Origin and petrogenetic implications. *Chemical Geology* **535**(2020), 11943. DOI: https://doi.org/10.1016/j.chemgeo.2020.119463

Berndt, J. & Klemmer, S. (2022) Origin of carbonatites – Liquid immiscibility caught in the act. *Nature Communications* **13**, 2892. DOI: https://doi.org/10.1038/s41467-022-30500-7

Biondi, J.C. & Braga, J.M. (2024) Main minerals of the Araxá alkali-carbonatite complex, Minas Gerais State, Brazil. *Journal of South American Earth Sciences* **134**(2024), 104751. DOI: https://doi.org/10.1016/jsames.2023.104751

Bohrson, W.A. & Spera, F.J. (2007) Energy constrained recharge, assimilation and fractional recrystallization (EC-RA*X*FC): A visual basic computer code for calculating trace element and isotopic variations of open system magmatic systems. *Geochemistry Geophysics Geosystems G3* **8**, Q11003. DOI: https://doi.org/10.1029/2007GC001781

Bohrson, W.A., Spera, F.J., Ghiorso, M.S., Brown, G.A., Creamer, J.B., & Mayfield, A. (2014) Thermodynamic model for energy-constrained open-system evolution of crustal magma bodies undergoing simultaneous recharge, assimilation and crystallization: The Magma Chamber Simulator. *Journal of Petrology* **55**, 1683–1717. DOI: https://doi.org/10.1093/petrology/eguo36

Bohrson, W.A., Spera, F.J., Heinonen, J.S., Brown, G.A., Scruggs, M.A., Adams, J.V., Takach, M.K., Zeff, G., & Suuikkanen, E. (2020) Diagnosing open-system magmatic processes using the Magma Chamber Simulator (MCS): Part I – Major elements and phase equilibria. *Contributions to Mineralogy and Petrology* **179**, 104. DOI: https://doi.org/10.1007/s00410-020-01722-s

Bouabdellah, M., Boukirou, W., Jebrak, M., Bogot, F., Yans, J., Mouttaqi, A., El Gadarri, M., Errami, A., & Levress, G. (2022) Discovery of antiskarn-hosted strategic metal mineralization in the Upper Cretaceous Twihinate carbonatite intrusion (West African Craton Margin, Moroccan Sahara). *Ore Geology Reviews* **149**, 1051056. DOI: https://doi.org/10.1016/j.oregeorev.2022.105105

Bowen, N.L. (1928) *The Evolution of the Igneous Rocks*. Dover Publications, New York, New York, USA.

Brod, J.A. (1999) *Petrology and Geochemistry of the Tapira Alkaline Complex, Minas Gerais State, Brazil.* PhD thesis. University of Durham, Durham, United Kingdom.

Brooker, R.A. & Kjarsgaard, B.A. (2011) Silicate-carbonate liquid immiscibility and phase relations in the system SiO_2–Na_2O–Al_2O_3–CaO–CO_2 at 0.1–2.5 GPa with applications to carbonatite genesis. *Journal of Petrology* **52**, 1281–1305.

Chakhmouradian, A.R., Mumin, A.H., Demény, A., & Elliot, B. (2008) Post-orogenic carbonatites at Eden Lake, Trans-Hudson Orogen (northern Manitoba): Geological setting, mineralogy and geochemistry. *Lithos* **103**(3–4), 503–526. DOI: https://doi.org./10.1016/j.lithos.2007.11.004

Chakhmouradian, A.R., Liu, Y., & Reguir, E.P. (2025) Uranium-rich pyrochlore, thorite and associated minerals in the Muluozhai rare-earth deposit (Sichuan, SW China): Implications for the geochemistry of high-field-strength elements in carbonatites and mineral exploration. *Mineralium Deposita* **60**(2025), 1537–1567. DOI: https://doi.org/10.1007/s00126-025-01357-9

Chmyz, L., Azzone, R.G., Ruberti, E., Marks, M.A.W., & Santos, T.J.S (2022) Olivines as probes into assimilation of silicate rocks by carbonatite magmas: Unravelling the genesis of reaction rocks from the Jacupiranga alkaline-carbonatite complex, southern Brazil. *Lithos* **416–417**, 106647.

Connolly, J.A.D. (1995) Phase diagram methods for graphitic rocks and applications to the system C–O–H–FeO–TiO_2–SiO_2. *Contributions to Mineralogy and Petrology* **119**, 94–116. DOI: https://doi.org/10.1007/bf0030720

Dalton, J.A. & Wood, B.J. (1993) The compositions of primary carbonate melts and their evolution through wall-rock reaction in the mantle. *Earth and Planetary Science Letters* **119**, 511–525.

Daly, R.A. (1910) Origin of alkaline rocks. *Bulletin of the Geological Society of America* **21**, 87–118.

Dasgupta, R., Hirschmann, M.M., & Smith, N.D. (2007) Partial melting experiments of peridotite + CO_2 at 3GPa and genesis of alkali ocean island basalts. *Journal of Petrology* **48**, 2093–2124.

de Capitani, C. & Petrakakis, K. (2010) The computation of equilibrium assemblage diagrams with Theriak-Domino software. *American Mineralogist* **95**, 1006–1016.

Franz, G.W. & Wyllie, P.J. (1966) Melting relationships in the system CaO–MgO–SiO_2–H_2O at 1 kilobar pressure. *Geochimica et Cosmochimica Acta* **30**, 9–22.

Genge, M.J., Price, P.G., & Jones, A.P. (1995) Molecular dynamic simulation of $CaCO_3$ melts to mantle pressures and temperatures: Implications for carbonatite magmas. *Earth and Planetary Science Letters* **131**, 225–238. DOI: https://doi.org/10.106/0012-8221X(95)00020-D

Ghiorso, M.S. & Gualda, G.A.R. (2015) An H_2O-CO_2 mixed fluid saturation model compatible with rhyolite-MELTS. *Contributions to Mineralogy and Petrology* **169**, 53. DOI: https://doi.org/10.1007/s00410-015-1141-8

Ghiorso, M.S. & Kelemen, P.B. (1987) Evaluating reaction stoichiometry in magmatic systems evolving under generalized thermodynamic constraints: Examples comparing isothermal and isenthalpic assimilation. *In* Magmatic processes: Physicochemical principles (B.O. Mysen, ed.). *Geochemical Society Special Publication* **1**, 319–336. ISBN: 0-941809-00-5.

Ghiorso, S. & Sack, O. (1995) Chemical mass transfer in magmatic processes. IV. A revised and internally consistent thermodynamic model for the interpolation and extrapolation of liquid–solid equilibria in magmatic systems at elevated temperatures and pressures. *Contributions to Mineralogy and Petrology* **119**, 197–212.

Giebel, R.J., Parsapoor, A., Walter, R.F., Braunger, S., Marks, M.A.W., Wenzel, T., & Markl, G. (2019) Evidence for magma-wallrock interaction in carbonatites from the Kaiserstuhl Volcanic Complex (Southwest Germany). *Journal of Petrology* **60**, 1163–1194.

Gittins, J. & Mitchell, R.H. (2023) The genesis of calcite and dolomite-forming magma by liquid immiscibility: A critical appraisal. *Geological Magazine* **160**, 1463–1480.

Grasso, C.R. (2010) Petrologia do complexo alkalino carbonatitico de Serra Negra. MG Dissertação (Mestrado em Geologia). Universidade de Brasilia, Brasilia, Brazil (157 pg.).

Green, D.H. & Wallace, M.E. (1988) Mantle metasomatism by ephemeral carbonatite melts. *Nature* **336**, 459–462. DOI: https://doi.org/10.1038/33459a0

Gualda, G.A.R., Ghiorso, M.S., Lemons, R.V., & Carley, T.L. (2012) Rhyolite-MELTS: A modified calibration of MELTS optimized for silica-rich, fluid-bearing magmatic systems. *Journal of Petrology* **53**, 875–890.

Gudelius, D., Marks, M.W., Markl, G., Nielson, T.F.D., Kolb, J., & Walter, B. (2023) The origin of ultramafic complexes with melilitolites and carbonatites: A petrological comparison of the Gardiner (E. Greenland) and Kovdor (Russia) intrusions. *Journal of Petrology* **64**, 1–2.

Gwalani, L.G., Avasia, R.K., Fernandez, S., & Chang, W.J. (1990) Sedimentological and petrological aspects of the Bagh sandstones of Dugdha-Naswadi (Amba Dongar carbonatite-alkalic complex) Gujarat. *Journal of the Indian Association of Sedimentologists* **9**, 21–28.

Heinonen, J.S., Iles, K.A., Heinonen, A., Fred, R., Virtanen, V.J., Bohrson, W.A., & Spera, F.J. (2020) Diagnosing open-system magmatic processes using the Magma Chamber Simulator (MCS): Part II – Trace elements and isotopes. *Contributions to Mineralogy and Petrology* **175**, 105. DOI: https://doi.org/10.1007/s00410-020-01718-9

Holland, T.J.B. & Powell, R. (2011) An improved internally consistent thermodynamic dataset for phases of petrological

interest, involving a new equation of state for solids. *Journal of Metamorphic Geology* **29**, 333–383.

Holmes, A. (1950) Petrogenesis of katungite and its associates. *American Mineralogist* **35**, 772–792.

Ju, N., Yang, G., Zhao, D., Wu, Y., Liu, B., Zhang, P., Liu, X., Shi, L., Feng, Y., Zhao, Z., Ren, Y., Wang, H., Yang, Q., Sun, Z., & Dong, S. (2025) Geology, mineralization and development potential of rare and uncommon earth ore deposits in Southwest China. *Minerals* **15**(5), 459. https://doi.org./10.3390/min15050459

King, B.C. (1949) The Napak area of southern Karamoja. *Memoirs of the Geological Survey of Uganda* **5**, 1–57.

Knudsen, C. (1985) Investigation of the Qaqarssuk carbonatite complex, southern West Greenland. *Grønlands Geologiske Undersøgelse* **125**, 34–40.

Krasnova, N.I., Balaganskaya, E.G., & Garcia, D. (2004) Kovdor – Classic phoscorites and carbonatites. *In* Phoscorites and Carbonatites from Mantle to Mine (F. Wall & A.N. Zaitsev, eds.). *Mineralogical Society of Great Britain and Ireland Series* **10**, 99–132. ISBN 0 903056 22 4.

le Roux, A. & Class, C. (2016) Metasomatic enrichment of Proterozoic mantle south of the Kaapvaal craton, South Africa: Origin of sinusoidal REE patterns in clinopyroxene and garnet. *Contributions to Mineralogy and Petrology* **171**, 14. DOI: https://doi.org/10.1007/s00410-015-1222-8

Liu, Y. & Anenburg, M. (2025) Reaction-driven magmatic crystallization at the Maoniuping carbonatite. *Nature Communications* **2025**(16), 7159. DOI: https://doi.org/10.1038/s41467-025-62009-0

Liu, Y., Hou, Z., Liu, H., Zheng, Z., & Luo, H. (2025) The magma source of the rare earth element-mineralized carbonatite syenite complexes in the Oligocene Mianning-Dechang belt, western Sichuan, Southwest China. *Lithos* **502–503**(2025), 108020.

Palmieri, M., Brod, J.A., Cordeiro, P., Gaspar, J.C., Barbosa, P.A.R., de Assis, L.C., Brod, T.C., Silva, S.E., Milanezi, B.P., Machadi, S.A., & Jacomo, M.H. (2022) The carbonatite related Morro do Padre niobium deposit, Catalão II complex, Central Brazil. *Economic Geology* **117**, 1497–1520. DOI: https://doi.org/10.5382/econgeo.4951

Patidar, R. & Agrawal, V. (2022) Emplacement of carbonatite and associate (*sic*) rocks of Siriwasan carbonatite complex, Gujarat: Evident (*sic*) by field relationship and petrology. *Journal of Scientific Research of Banares University* **66**, 1–10. DOI: https://doi.org/10.37398/JSR.2022.660301

Pdah, D.S.M. & Khonglah, M.A. (2022) Orbicular and nodular structures in carbonatite of the Sung Valley ultramafic-alkaline-carbonatite complex, Shillong Plateau, Meghalaya, NE India: Their petrogenetic implications. *Journal of the Geological Society of India* **98**, 635–640. DOI: https://doi.org/10.1007/s12594-022-2038-6

Powell, R. & Holland, T.J.B. (1988) An internally consistent dataset with uncertainties and correlations: 3 Applications to geobarometry, worked examples and a computer program. *Journal of Metamorphic Geology* **6**, 173–205.

Riel, N., Kaus, B.J.P., Green, E.C.R., & Berlie, N. (2022) MAGEMIN, an efficient Gibbs energy minimizer: Application to igneous systems. *Geochemistry, Geophysics, Geosystems* **23**, e2022GC010427.

Rimskaya-Khorskova, O.M. & Krasnova, N.I. (2002) *Geology of the Deposits of Kovdor Massif.* St. Petersburg University Press, St. Petersburg, Russia (146 pg.) (in Russian). ISBN 5-288-02859-1.

Savard, J.J. & Mitchell, R.H. (2021) Petrology of ijolite series rocks from the Prairie Lake (Canada) and Fen (Norway) alkaline rock carbonatite complexes. *Lithos* **396–397**, 101688.

Schmidt, M.W., Guiliani, A., & Poli, S. (2024) The origin of carbonatites – Combining the rock record with available experimental constraints. *Journal of Petrology* **2024**, egae105. DOI: https://doi.org/10.1093/petrology/egae105

Schuiling, R.D. (1964) The limestone assimilation hypothesis. *Nature* **204**, 1054–1055.

Secher, K. & Larsen, L.M. (1980) Geology and mineralogy of the Sarfartôq carbonatite complex, southern West Greenland. *Lithos* **13**, 199–212.

Smithies, R.H. & Marsh, J.S. (1998) The Marinkas Quellen carbonatite complex, southern Namibia: Carbonatite magmatism with an uncontaminated depleted mantle signature in a continental setting. *Chemical Geology* **148**, 201–212.

Spera, F.J. & Bohrson, W.A. (2001) Energy-constrained open-system magmatic processes I: General model and energy-constrained assimilation and fractional crystallization (EC-AFC) formulation. *Journal of Petrology* **42**, 999–1018.

Spera, F.J. & Bohrson, W.A. (2002) Energy-constrained open-system magmatic processes 3: Energy-constrained assimilation and fractional crystallization (EC-AFC). *Geochemistry Geophysics Geosystems G3*^{3} **3**, 8001. DOI: https://doi.org/10.1029/2002GC00315

Spera, F.J. & Bohrson, W.A. (2004) Open-system magma chamber evolution: An energy-constrained geochemical model incorporating the effects of concurrent eruption, recharge, variable assimilation and fractional crystallization (EC-E′RA$_\chi$FC). *Journal of Petrology* **45**, 2459–2480. DOI: https://doi.org.10.1093/petrology/egh072

Su, K., Zhang, S.-B., Li, Z.-X., Zhan, L., Liang, T., Du, Y., & Li, L. (2023) When carbonatite met granite: A carbonatite magma–wall rock reaction origin for the Paleoproterozoic pyroxenite and syenite in Fengzhen, North China. *Lithos* **454–455**(2023), 107231.

Taylor, H.P. Jr. (1980) The effects of assimilation of country rocks by magmas on $^{18}O/^{16}O$ and $^{87}Sr/^{86}Sr$ systematics in

igneous rocks. *Earth and Planetary Science Letters* **47**, 243–254.

Tomkute, V., Solheim, A., Sakirzanovas, B., Øye, B., & Olsen, E. (2014) Phase equilibria evaluation for CO_2 capture: CaO–CaF_2–NaF; $CaCO_3$–NaF–CaF_2; and Na_2CO_3–CaF_2NaF. *Journal of Chemical and Engineering Data* **59**, 1257–1263.

Vasyukova, O.V. & Williams-Jones, A.E. (2022) Carbonatite metasomatism, the key to unlocking the carbonatite-phoscorite-ultramafic rock paradox. *Chemical Geology* **602**, 120888.

Vasyukova, O.V., Kostyuk, A., & Williams-Jones, A.E. (2022) Kovdor to Oldoinyo Lengai – The missing link in carbonatitic magma evolution. *Geology* **51**, 59–63.

Veksler, I.V., Nielson, T.F.D., & Sokolov, S.V. (1998) Mineralogy of crystallized melt inclusions from Kovdor and Gardiner ultramafic alkaline complexes: Implications for carbonatite petrogenesis. *Journal of Petrology* **39**, 2015–2031.

von Eckermann, H. (1950) A comparison between the parageneses of Fennoscandian limestone contact minerals and those of the Alnö alkaline rocks, associated with carbonatites. *Mineralogical Magazine* **29**, 304–312. DOI: https://doi.org/10.11180/minmag.1950.029.211.07

Walter, B.F., Giebel, R.J., Marlow, A.G., Siegfried, P.R., Marks, M., Markl, G., Palmer, M., & Kolb, J. (2022) The Kieshöhe carbonatites of southwestern Namibia: The post-magmatic role of silicate xenoliths on REE mobilisation. *Communications Geological Survey of Namibia* **3**, 1–31.

Weidendorfer, D., Schmidt, M.W., & Mattsson, H.B. (2017) A common origin of carbonatite magmas. *Geology* **45**(6), 507–510. DOI: https://doi.org/10.1130/G388801.1

Williams-Jones, A.E. & Vasyukova, O.V. (2023) Niobium, critical metal, and progeny of the mantle. *Economic Geology* **118**, 837–855.

Wyllie, P.J. & Lee, P.J. (1998) Model system controls on conditions of formation of magnesiocarbonatite and calciocarbonatite magmas rom the mantle. *Journal of Petrology* **39**, 1885–1893. DOI: https://doi.org/10.1093/petroj/39.11-12.1885

Wyllie, P.J. & Watkinson, D.H. (1970) Phase equilibrium studies bearing on genetic links between alkaline and subalkaline magmas, with special reference to the limestone assimilation hypothesis. *The Canadian Mineralogist* **10**, 362–374.

Yaxley, G.M., Anenburg, M., Tappe, S., Decree, S., & Guzmics, T. (2022) Carbonatites: Classification, sources, evolution and emplacement. *Annual Reviews of Earth and Planetary Sciences* **50**, 261–293.

Yin, S., Xie, Y., & Liang, Y. (2021) A review of REE enrichment and fractionation mechanism during magma evolution of ore-forming carbonatite and significance of mineral zonation in carbonatite. *Mineralium Deposita* **40**, 949–962.

Xiao, Y., Wang, W., Yang, X., Cao, Y., Than, P., & Zhao, Z. (2025) Mineralogical fingerprints of crustal silica contamination in the Bayan Obo carbonatite. *American Mineralogist* **110**, 452–466.

Xu, C., Chakhmouradian, A.R., Kynicky, J., Li, Y., Song, W., & Chen, W. (2019) A Paleoproterozoic mantle source modified by subducted sediments under the North China craton. *Geochimica et Cosmochimica Acta* **245**, 222–239.

Zheng, X., Liu, Y., Smith, M.P., Kynicky, J., & Hou, Z. (2023) Carbonatitic magma fractionation and contamination generate rare earth element enrichment and mineralization in the Maoniuping giant REE deposit, SW China. *Journal of Petrology* **64**, 1–36.

Received December 3, 2025. Revised manuscript accepted May 5, 2026.

This manuscript was handled by Associate Editor Leo Millonig and Editor Stephen Prevec.

APPENDIX 1

The development begins by defining expressions for the enthalpy, h(T) valid in subsolidus, melting range, and superliquidus temperature intervals for each endmember. These expressions are based upon initial temperatures, their respective solidii and liquidii and thermal properties including fusion enthalpies. The temperature intervals of interest are shown in Figure 1 and depend on the ordering of solidii and liquidii for the endmembers. The energy balances depend upon the temperature line order, specifically the relative solidii and liquidii, depicted in Figure 1.

The enthalpy-temperature relations for wallrock (subscript 'g' for granite) in each relevant temperature interval are:

$$h_g(T) = m_g C_{sg}(T - T_{og}) \text{ in the temperature interval } T_{og} \le T \le T_{Sg} \quad \text{(A1)}$$

$$h_g(T) = m_g\left\{C_{sg}(T_{Sg} - T_{og}) + \frac{(T - T_{Sg})}{(T_{Lg} - T_{Sg})}\left[C_{\ell g}(T - T_{Sg}) + \Delta h_{fg}\right] + \frac{(T_{Lg} - T)}{(T_{Lg} - T_{Sg})}\left[C_{sg}(T - T_{Sg})\right]\right\}$$

for the wallrock in the melting interval, $T_{Sg} \le T \le T_{Lg}$ (A2)

and

$$h_g(T) = m_g\{C_{sg}(T_{Sg} - T_{og}) + C_{\ell g}(T_{Lg} - T_{Sg}) + \Delta h_{fg} + C_{\ell g}(T - T_{Lg})\}$$

at wallrock superliquidus conditions $T_{Lg} \le T \le T_{oc}$ (A3).

In Equation (A2) a linear relationship between melt fraction and temperature has been assumed in the melting interval where melt fractions are explicitly written in terms of temperature:

$$\phi_\ell = (T - T_{Sg})/(T_{Lg} - T_{Sg}) \text{ and } \phi_s = (T_{Lg} - T)/(T_{Lg} - T_{Sg}) \quad \text{(A4).}$$

For the carbonatite endmember, the enthalpy-temperature relations in each interval are:

$$h_c(T) = m_c C_{\ell c}(T - T_{oc}) \text{ in the temperature range } T_{Lc} \le T \le T_{oc} \quad \text{(A5)}$$

$$h_c(T) = m_c\left\{C_{\ell c}(T_{Lc} - T_{oc}) + \frac{(T - T_{Sc})}{(T_{Lc} - T_{Sc})}\left[C_{\ell c}(T - T_{Lc})\right] + \frac{(T_{Lc} - T)}{(T_{Lc} - T_{Sc})}\left[C_{sc}(T - T_{Lc}) - \Delta h_{fc}\right]\right\}$$

in the temperature range $T_{Sc} \le T \le T_{Lc}$ (A6)

and

$$h_c(T) = m_c\{C_{sc}(T_{Sc} - T_{Lc}) - \Delta h_{fc} + C_{\ell c}(T_{Lc} - T_{oc}) + C_{sc}(T - T_{Sc})\}$$

at carbonatite subsolidus conditions $T_{og} \le T \le T_{Sc}$ (A7).

All parameters are defined in Table 2 in the text. In (A6) a linear relationship between melt

fraction and temperature has been assumed according to (A4) but where solidus and liquidus temperatures refer to the carbonatitic endmember. Non-linear relations between melt and solid fractions could be used without affecting the development although the solutions become algebraically more cumbersome.

Examination of enthalpy relations reveals that the parameters in (A1-A7) include the initial temperature, solidus and liquidus, fusion enthalpy and isobaric heat capacities of solid and melt for each endmember. Typical numerical values appropriate for assimilation of granitic wallrock by hotter carbonatitic magma are collected in Table 1 in the text. Numerical values for these parameters are required to define a solution. Once a temperature line (figure 1a-d) is chosen then numerical value must honor that ordering. For most of what follows the ordering of Figure 1a is followed. The particular ordering used is always defined in numerical results.

The final common temperature of the mixed wallrock-magma system formed by isenthalpic assimilation is found by setting the sum of the enthalpies of wallrock and carbonatitic magma equal to a constant, that is

$$h_g + h_c = \mathcal{C} \qquad \text{(A8)}$$

and solving for the final temperature T_f, at thermal equilibrium. The constant $\mathcal{C}$ is determined from the initial condition (before mixing) when $T_g=T_{og}$ and $T_c=T_{oc}$. Using (A1) and (A5) and the initial temperatures, one finds $\mathcal{C} = 0$, which is the mathematical statement that defines the initial (pre-mixing) and hence final post-assimilation enthalpy of the system. Enthalpy is exchanged between endmembers during thermal equilibration under the constraint of constant enthalpy; that is, the final mixed state is identical to the sum of the endmember enthalpies before 'mixing'.

Examination of Figure 1 reveals that there are five coterminous temperature intervals where T_f may be found depending on the specific h(T) relation for each endmember applicable in each relevant temperature interval. For example, if T_f lies in the subsolidus range $T_{og} \le T \le T_{Sg}$ then (see figure 1) enthalpy constancy requires equating (A1) and (A5):

$$h_g(T) + h_c(T) = m_g C_{sg}(T - T_{og}) + m_c\{C_{sc}(T_{Sc} - T_{Lc}) - \Delta h_{fc} + C_{\ell c}(T_{Lc} - T_{oc}) + C_{sc}(T - T_{Sc})\} = 0 \qquad \text{(A9)}$$

This expression is interpreted as follows: for any equilibrated temperature (T_f) in the range $T_{og} \le T \le T_{Sg}$ the condition expressed by (A9) for isenthalpic assimilation must hold. Note that the mass of wallrock (m_g) and of carbonatitic melt (m_c) appear explicitly in (A9). Dividing both sides by m_g, the mixing ratio, defined $\mathcal{R} = m_c/m_g$, can be determined as a function of any final temperature in the range $T_{og} \le T_f \le T_{Sg}$ by rearrangement of (A9) using the definition of $\mathcal{R}$. The result is

$$\mathcal{R} = \frac{C_{sg}(T_{og} - T_f)}{C_{sc}(T_{Sc} - T_{Lc}) - \Delta h_{fc} + C_{\ell c}(T_{Lc} - T_{oc}) + C_{sc}(T_f - T_{Sc})} \qquad \text{(A10).}$$

Now, the temperature interval bounds can be used to determine the bounding values for $\mathcal{R}$. At $T_f=T_{og}$, $\mathcal{R} = 0$ since this is the trivial case of no mixing. At the upper bound of this interval $T_f=T_{Sg}$ (see Figure 1). From A(10) using the parameters of table 1 find that $\mathcal{R} = \mathcal{R}_{max} = 0.288$. Recall that $f_c = \mathcal{R}/(1 + \mathcal{R})$ and hence $\mathcal{R}_{max}$ determines the maximum fraction of carbonatitic magma of the mixture in the isenthalpic assimilation process such that the final temperature falls at the granite solidus, T_{Sg}. In this case, $f_{c\ max}= 0.224$. That is, for mass fractions of carbonatite in

the mixture between zero and 0.224, T_f will lie between T_{og}, the initial temperature of wallrock and T_{Sg} the granite solidus of 600 ℃ (Table 1). Stated differently, if the fraction of carbonatitic magma in the mixture is less than ~ 22% by mass, the final temperature after isenthalpic mixing will not exceed the granite solidus. The system is 'choked' by the cold wallrock and the end product is crystallized carbonatitic magma and subsolidus granite. There is not sufficient enthalpy in the combined endmembers to give a final temperature after interaction exceeding that of the granite solidus.

Examination of Figure 1a reveals that there are four additional temperature intervals for which the range of $\mathcal{R}$ and hence $f_{c\ max}$ can be determined. These results are summarized in Table A1a. Finally, in Table A2 the relationship between $\mathcal{R}$ and temperature for the parameters of Table 1 are given. From Table A1a one can determine the temperature range that any given mass ratio corresponds to. For example, for a carbonatite -granite interaction with a mass ratio $\mathcal{R} = \frac{m_c}{m_g} = 1$, from Table A1a the final T must lie between the carbonatite solidus T_{Sc} and wallrock liquidus T_{Lg}. The final temperature T_f within this interval is found by using the appropriate eqs listed in Table A1a for the relevant temperature range indicated and the chosen value of $\mathcal{R}$. Following this method, the Figure 2 in the text gives results for temperatures across the entire range from initial temperature of the wallrock to the initial temperature of carbonatitic magma. The expressions are provided in Table A2.

Isenthalpic thermal model: Incorporation of reaction enthalpies

There are many potential reactions to consider when carbonatitic magma reacts with silicate phases in wallrock. Comprehensively accounting for all possibilities requires implementation of a multicomponent-multiphase thermodynamic model). Unfortunately, extant codes cannot handle phase relations across the entire compositional spectrum for *isenthalpic processes*. Here we consider representative reactions between carbonate and silicate phases. It is emphasized that the reactions listed are not exhaustive. For the purposes of this study, it is important to examine the energetics of typical reactions enumerated by the index j with j={1, 2, 3,…,16}

(1) $CaCO_{3\ (m)} + SiO_{2\ (qtz)} === CaSiO_{3\ (wo)} + CO_{2\ (g)}$

(2) $CaCO_{3\ (m)} + NaAlSi_30_{8\ (ab)} === CaSiO_{3\ (wo)} + NaAlSi_2O_{6\ (jd)} + CO_{2\ (g)}$

(3) $CaCO_{3\ (m)} + CaAl_2Si_20_{8\ (an)} === CaSiO_{3\ (wo)} + CaAl_2SiO_{6\ (Ca\text{-}ts)} + CO_{2\ (g)}$

(4) $MgCO_{3\ (m)} + SiO_{2\ (qtz)} === MgSiO_{3\ (en)} + CO_2$

(5) $MgCO_{3\ (m)} + NaAlSi_30_{8\ (ab)} === MgSiO_{3\ (en)} + NaAlSi_2O_{6\ (jd)} + CO_{2\ (g)}$

(6) $MgCO_{3\ (m)} + CaAl_2Si_20_{8\ (an)} === MgSiO_{3\ (en)} + CaAl_2SiO_{6\ (Ca\text{-}ts)} + CO_{2\ (g)}$

(7) $CaMg(CO_3)_{2\ (m)} + 2SiO_{2\ (qtz)} === CaMgSi_2O_{6\ (di)} + 2CO_2$

(8) $CaMg(CO_3)_{2\ (m)} + 2SiO_{2\ (qtz)} === CaSiO_{3\ (wo)} + + MgSiO_{3\ (en)} + 2CO_2$

(9) $CaMg(CO_3)_{2\ (m)} + 2\ NaAlSi_30_{8\ (ab)} === CaMgSi_2O_{6\ (di)} + 2NaAlSi2O_{6\ (jd)} + 2CO_2$

(10) $CaMg(CO_3)_{2\ (m)} + 2\ NaAlSi_30_{8\ (ab)} === CaSiO_{3\ (Wo)}) + MgSiO_{3\ (En)} + 2NaAlSi2O_{6\ (jd)} + 2CO_{2\ (g)}$

(11) $CaMg(CO_3)_{2\,(m)}$+2 $CaAl_2Si_20_{8\,(an)}$ === $CaMgSi_2O_{6\,(di)}$ +2 $CaAl_2SiO_{6\,(Ca\text{-}ts)}$ + $2CO_2$

(12) $CaMg(CO_3)_{2\,(m)}$+ $2CaAl_2Si_20_{8\,(an)}$ == $CaSiO_{3\,(Wo)}$ + $MgSiO_{3\,(En)}$+ $2CaAl_2SiO_{6\,(Ca\text{-}ts)}$ + $2CO_{2\,(g)}$

(13) $FeCO_{3\,(m)}$ + $SiO_{2\,(qtz)}$ =====$FeSiO_{3(fs)}$+ $CO_{2\,(g)}$

(14) $K_2CO_{3\,(m)}$ +$5SiO_{2\,(qtz)}$ + $CaAl_2Si_2O_{8\,(an)}$ ===$2KAlSi_3O_{8\,(or)}$ + $CaSiO_{3\,(wo)}$ + $CO_{2\,(g)}$

(15) $Na_2CO_{3\,(m)}$ +$5SiO_{2\,(qtz)}$ + $CaAl_2Si_2O_{8\,(an)}$===$2NaAlSi_3O_{8\,(or)}$ + $CaSiO_{3\,(wo)}$ + $CO_{2\,(g)}$

(16) $Na_2CO_{3\,(m)}$+ $NaAlSiO_{4\,(ne)}$+ $MgSiO_{3\,(en)}$+$6CaAl_2Si_2O_{8\,(an)}$ ==

$NaAlSi_3O_{8\,(ab)}$+$2NaAlSi_2O_{6\,(jd)}$ +$CaMgSi_2O_{6\,(di)}$ + $5CaAl_2SiO_{6\,(Ca\text{-}ts)}$ + $CaMgSi_2O_{6\,(di)}$ + $CO_{2\,(g)}$

The common feature of these reactions is that carbonatitic magma (written in terms of a single component) reacts with wallrock silicates to form other silicates (mainly pyroxenes) and liberate CO_2. Reactions in which alkali amphiboles are stable can also be written. At crustal pressures and magmatic temperatures these reactions possess negative Gibbs energies and hence are spontaneous. Values of the enthalpy, entropy, isobaric heat capacity and volume change for these reactions are given in Table A2. All reactions are endothermic in the reference state of 1 bar and 298 K roughly equaling ~10^5 J per mol of carbonate reactant. Reaction heat capacities are small and negative whereas reaction enthalpies are all large and positive, typical of reactions in which a gas, CO_2 in this case, is liberated. The volume change of the solids for all reactions is negative. Collected in Table A2 are the critical mass ratios of carbonate and silicate phase reactants for each reaction. Recall that these ratios are defined for each reaction by the reaction stoichiometry. When the reactants are in the mass ratio $\mathcal{R}_c^*$ then neither carbonate nor silicate reactant is limiting and the heat absorbed is at a maximum. Values in Table A2 have been used to compute the Gibbs energies and enthalpies of reaction (j=1,2,3,… 13) at high temperatures and 200 MPa (2 kilobars) that are collected in Table A3. The reactions are spontaneous and endothermic at magmatic temperatures at depths corresponding to the upper crust. That is, heat must be supplied during assimilation to bring the reactants to magmatic temperatures as outlined earlier. Heat is consumed in these decarbonation reactions and this puts an additional thermal burden on the high temperature thermal reservoir (carbonatitic magma) that to supply heat to wallrock and drive the reactions. Evaluation of the reaction enthalpies for typical reactions at appropriate upper crustal pressures and temperatures ($700℃ - 1100℃$) reveals values around +1000 kJ per kg of carbonate reactant. These values exceed typical fusion enthalpies for silicates. One anticipates, consequently, that the limits of model 1 will move in a direction to make reaction of carbonate with wallrock silicates less likely in the sense that the ratio $\mathcal{R} = m_c/m_g$ will be higher to achieve any given thermally equilibrated temperature.

From examination of the stoichiometry of specific decarbonation reactions the enthalpy requirement for the reaction to run to completion depends on the mass fraction f_c^* of the carbonate in the reactant mixture as defined by the reaction stoichiometry. This criterion can also be translated to the mass ratio $\mathcal{R}^* = m_c^*/m_g^*$. The maximum heat consumption takes place when the carbonate to silicate ratio is in the optimal proportion defined by the reaction stoichiometry. For example, adopting reaction (1) for illustration, the maximum consumption of enthalpy occurs when the fraction of carbonate in the reactant mixture or, as an alternative description, the mass ratio are respectively

$$f_c^* = M_{cc}\,\nu_{cc}/(M_{cc}\nu_{cc} + M_{qtz}\,\nu_{qtz}) \quad \text{or} \quad \mathcal{R}_c^* = M_{cc}\,\nu_{cc}/(M_{qtz}\,\nu_{qtz}) \qquad \text{(A11)}$$

where M is the molar mass of the subscripted phase (i.e., for reaction *j*=1, calcite or quartz in this example) and ν represents the stoichiometric coefficients of the respective reactants. For this reaction, f_c^*=0.62 or, cast as a ratio, $\mathcal{R}^* = \frac{m_c^*}{m_g} = 1.666$. (see table A2). When calcite and quartz are in mass ratio 1.67, the enthalpy requirement for consumption of all reactant is at a maximum. When calcite is the limiting reactant $\mathcal{R} < \mathcal{R}^*$ since there is insufficient carbonate to react with excess quartz and when $\mathcal{R} > \mathcal{R}^*$ quartz is the limiting reactant (excess carbonate). Each reaction defines a unique and optimal $\mathcal{R}_j^*$ where the subscript *j* is indexed to a particular reaction (1)-(16) above. Numerical values are provided in Table A3.

The enthalpy requirement for each reaction depends on which reactant is limiting:

$$\Delta h_{rxn} = \Delta h_{jc}^* \, m_c \quad \text{for } \mathcal{R} < \mathcal{R}^* \qquad \text{(A12)}$$

or

$$\Delta h_{rxn} = \Delta h_{jc}^* \, \frac{\mathcal{R}^*}{\mathcal{R}} \, m_c \quad \text{for } \mathcal{R} > \mathcal{R}^* \qquad \text{(A13).}$$

In (A12) and (A13), Δh_{jc}^* represents the enthalpy of the j^{th} reaction per kg of carbonate reactant. The key aspect is that at fixed pressure these reactions exhibit a temperature-dependent reaction enthalpy that is maximal when the mass ratio of reactant carbonate to reactant silicate is in the ratio defined by the reaction stoichiometry.

Isenthalpic thermal model: Enthalpy balance expressions

In order to incorporate reactions, eqs(A1)-(A7) are modified to include reaction enthalpies. The value of $\mathcal{R}^*$ depends on the specific reaction and is indexed according to $\mathcal{R}_j^*$ where the index j refers to the reaction number $j = \{1, 2, 3, \ldots 11\}$ and the asterisk reminds one that this mass ratio is the one defined uniquely for each reaction by its stoichiometry. The temperature intervals used here are identical to those used in the simple thermal model (see Figure 1 and Table 2a).

The expressions for enthalpy, h(T) for the endmembers are modified to account for the endothermic quality of the reactions. h(T) expressions are valid in each range of temperature indicated. The effects of reaction enthalpy are included with the 'granite' endmember since the endothermic reactions are a heat sink with the required energy being supplied by the initially hotter carbonatitic magma. There are now two expressions for the enthalpy of the wallrock granite endmember: one for $\mathcal{R} < \mathcal{R}^*$ and one for $\mathcal{R} > \mathcal{R}^*$. The enthalpy-temperature relations in each of the relevant temperature intervals are:

For final (equilibrated) temperatures in the range $T_{og} \le T \le T_{Sg}$ if $\mathcal{R} < \mathcal{R}^*$

$$h_g(T) = m_g C_{sg}\left(T - T_{og}\right) + \Delta h_{jc}^* \, m_c \qquad \text{(A14a)}$$

whereas

$$h_g(T) = m_g C_{sg}\left(T - T_{og}\right) + \Delta h_{jc}^* \, \frac{\mathcal{R}^*}{\mathcal{R}} \, m_c \quad \text{if } \mathcal{R} > \mathcal{R}^* \qquad \text{(A14b).}$$

For final (equilibrated) temperatures in the range $T_{Sg} \le T \le T_{Lg}$ if $\mathcal{R} < \mathcal{R}^*$ is

$$h_g(T) = m_g\left(C_{ŝg}(T_{Sg} - T_{og}) + \frac{(T-T_{Sg})}{(T_{Lg}-T_{Sg})}\left[C_{\ell g}(T - T_{Sg}) + \Delta h_{fg}\right] + \frac{(T_{Lg}-T)}{(T_{Lg}-T_{Sg})}\left[C_{ŝg}(T - T_{Sg})\right]\right) + \Delta h^*_{jc}\, m_c$$

(A15a)

whereas

$$h_g(T) = m_g\left(C_{ŝg}(T_{Sg} - T_{og}) + \frac{(T-T_{Sg})}{(T_{Lg}-T_{Sg})}\left[C_{\ell g}(T - T_{Sg}) + \Delta h_{fg}\right] + \frac{(T_{Lg}-T)}{(T_{Lg}-T_{Sg})}\left[C_{ŝg}(T - T_{Sg})\right]\right) + \Delta h^*_{jc}\,\frac{\mathcal{R}^*}{\mathcal{R}}\, m_c \quad \text{(A15b)}$$

if $\mathcal{R} > \mathcal{R}^*$

Finally, in the temperature range $T_{Lg} \le T \le T_{oc}$ if $\mathcal{R} < \mathcal{R}^*$

$$h_g(T) = m_g\left(C_{ŝg}(T_{Sg} - T_{og}) + C_{\ell g}(T_{Lg} - T_{Sg}) + \Delta h_{fg} + C_{\ell g}(T - T_{Lg})\right) + \Delta h^*_{jc}\, m_c$$

(A16a)

whereas

$$h_g(T) = m_g\left(C_{ŝg}(T_{Sg} - T_{og}) + C_{\ell g}(T_{Lg} - T_{Sg}) + \Delta h_{fg} + C_{\ell g}(T - T_{Lg})\right) + \Delta h^*_{jc}\,\frac{\mathcal{R}^*}{\mathcal{R}}$$

if $\mathcal{R} > \mathcal{R}^*$ (A16b).

The final temperature of the wallrock-magma mixture formed at constant enthalpy but allowing for reaction between molten carbonate and granitic wallrock is found by setting the sum of the enthalpies of granitic host and carbonatitic magma equal to a constant (the isenthalpic constraint) and solving for the final temperature T_f of the thermally equilibrated mixture for a given mass ratio. The constant $\mathcal{C}$ is determined at the initial condition (before mixing) when T_g=T_{og} and T_c=T_{oc}. Examination of Figure 1 reveals that there are five coterminous temperature intervals where T_f may be found depending on the specific h(T) relation for each endmember that is applicable in each prescribed temperature interval. For the granite endmember, the endothermic heat sink depends numerically on whether the mixing ratio $\mathcal{R} < \mathcal{R}^*$ or $\mathcal{R} > \mathcal{R}^*$. As an example, if T_f lies in the range $T_{og} \le T \le T_{Sg}$ (figure 1) then appropriate balance is found by equating eqs (A14a) and (A7) for $\mathcal{R} < \mathcal{R}^*$

$$h_g(T) + hc(T) = m_g C_{ŝg}(T - T_{og}) + \Delta h^*_{jc}\, m_c + m_c\{C_{ŝc}(T_{Sc} - T_{Lc}) - \Delta h_{fc} + C_{\ell c}(T_{Lc} - T_{oc}) + C_{ŝc}(T - T_{Sc})\} = 0$$

(A17a)

or

$$h_g(T) + hc(T) = m_g C_{ŝg}(T - T_{og}) + +\Delta h^*_{jc}\,\frac{\mathcal{R}^*}{\mathcal{R}}\, m_c + m_c\{C_{ŝc}(T_{Sc} - T_{Lc}) - \Delta h_{fc} + C_{\ell c}(T_{Lc} - T_{oc}) + C_{ŝc}(T - T_{Sc})\} = 0$$

(A17b)

if $\mathcal{R} > \mathcal{R}^*$).

This expression is interpreted as follows: for any final temperature in the range $T_{og} \le T \le T_{Sg}$

the condition expressed by eqs (A17a or b) for isenthalpic mixing must hold. Note that the mass of wallrock (m_g) and of carbonatitic melt (m_c) appear explicitly.

Using eq (A17a) as an example the mixing ratio, $\mathcal{R} = \frac{m_c}{m_g}$ can be found as a function of temperature T_f in the range $T_{og} \leq T \leq T_{Sg}$. Rearrangement of eq (A17b) and using (A13) for $\mathcal{R} > \mathcal{R}^*$ when carbonate is the limiting reactant gives

$$\mathcal{R} = \frac{C_{sg}(T_{og}-T)-\Delta h_j^* \mathcal{R}_j^*}{C_{sc}(T_{Sc}-T_{Lc})-\Delta h_{fc}+C_{\ell c}(T_{Lc}-T_{oc})+C_{sc}(T-T_{Sc})} \qquad \text{(A18)}$$

At T= $T_{Sg}$the upper bound for $\mathcal{R}$ is 1.82. Adopting reaction 1 as an example to illustrate the method, since the critical mass ratio is (see Table A2) $\mathcal{R}_c^* = 1.67$, eq (A18) is the correct enthalpy balance. T_f will lie between T_{og} , the initial temperature of wallrock and T_{Sg} the granite solidus of 600 ℃ (Table 1). Stated equivalently, if the fraction of carbonatitic magma in the mixture is less 0.65, then the final temperature after isenthalpic mixing will not exceed the granite solidus. The system is 'choked' by the cold wallrock and the end product is crystallized carbonatitic magma and subsolidus granite. In the immediate vicinity of the boundary calc-silicate phases would appear (e.g., Evans, 2007).

The diagrams in the text were determined by the methods given in this Appendix.

APPENDIX TABLES

Table A1a. Range of mass ratio and mass fractions are based on parameters defined in Table 2 (text) for the temperature ordering ($T_{og}<T_{Sg}<T_{Sc}<T_{Lg}<T_{Lc}<T_{oc}$). Property values correspond to set 2 (Table 2 text).

Temperature range	h(T) equations		Range of mixing ratio $\mathcal{R}$	Range of mass fraction carbonatite fc in mixture
	granite	carbonatite		
$T_{og} \le T_f \le T_{Sg}$	eq (A1)	eq (A7)	$0 \le \mathcal{R} \le 0.288$	$0 \le f_c \le 0.224$
$T_{Sg} \le T_f \le T_{Sc}$	eq (A2)	eq (A7)	$0.288 \le \mathcal{R} \le 0.534$	$0.224 \le f_c \le 0.348$
$T_{Sc} \le T_f \le T_{Lg}$	eq (A2)	eq (A6)	$0.534 \le \mathcal{R} \le 6.958$	$0.348 \le f_c \le 0.874$
$T_{Lg} \le T_f \le T_{Lc}$	eq (A3)	eq (A6)	$6.958 \le \mathcal{R} \le 17.679$	$0.874 \le f_c \le 0.946$
$T_{Lc} \le T_f \le T_{oc}$	eq (A3)	eq (A5)	$17.679 \le \mathcal{R} < \infty$	$0.946 \le f_c \le 1$

Table A1b. Enthalpy expressions based on temperature ordering $T_{og}< T_{Sc}< T_{Sg}<T_{Lg}<T_{Lc}<T_{oc}$.

Temperature range	h(T) equations	
	granite	carbonatite
$T_{og} \le T_f \le T_{Sc}$	eq (A1)	eq (A7)
$T_{Sc} \le T_f \le T_{Sg}$	eq (A1)	eq (A6)
$T_{Sg} \le T_f \le T_{Lg}$	eq (A2)	eq (A6)
$T_{Lg} \le T_f \le T_{Lc}$	eq (A3)	eq (A6)
$T_{Lc} \le T_f \le T_{oc}$	eq (A3)	eq (A5)

Table A1c. Enthalpy expressions based on temperature ordering $T_{og}< T_{Sc}< T_{Sg}< T_{Lc} < T_{Lg} <T_{oc}$.

Temperature range	h(T) equations)	
	granite	carbonatite
$T_{og} \le T_f \le T_{Sc}$	eq (A1)	eq (A7)
$T_{Sc} \le T_f \le T_{Sg}$	eq (A1)	eq (A6)
$T_{Sg} \le T_f \le T_{Lc}$	eq (A2)	eq (A6)
$T_{Lc} \le T_f \le T_{Lg}$	eq (A2)	eq (A5)

Table A1d. Enthalpy expressions based on temperature ordering $T_{og}< T_{Sg}< T_{Sc}< T_{Lc} < T_{Lg} <T_{oc}$.

Temperature range	h(T) equations	
	granite	carbonatite
$T_{\mathrm{og}} \leq T_f \leq T_{Sg}$	eq (A1)	eq (A7)
$T_{\mathrm{Sg}} \leq T_f \leq T_{Sc}$	eq (A2)	eq (A7)
$T_{\mathrm{Sc}} \leq T_f \leq T_{Lc}$	eq (A2)	eq (A6)
$T_{\mathrm{Lc}} \leq T_f \leq T_{Lg}$	eq (A2)	eq (A5)
$T_{\mathrm{Lg}} \leq T_f \leq T_{oc}$	eq (A3)	eq (A5)

Table A2. Formulae defining mass ratio versus temperature relations

Temperature Range	$\mathcal{R}$ vs T relation
$T_{og} \leq T \leq T_{Sg}$	$\mathcal{R}_1 = \dfrac{\mathrm{C_{sg}(T_{og} - T)}}{\mathrm{C_{sc}(T_{Sc} - T_{Lc}) - \Delta h_{fc} + C_{\ell c}(T_{Lc} - T_{oc}) + C_{sc}(T - T_{Sc})}}$
$T_{Sg} \leq T \leq T_{Sc}$	$\mathcal{R}_2 = \dfrac{\mathrm{C_{sg}\left(T_{og} - T_{Sg}\right) + \left(\frac{T_{Sg} - T}{T_{Lg} - T_{Sg}}\right)\left[C_{\ell g}\left(T - T_{Sg}\right) + h_{fg}\right] + \left(\frac{T - T_{Lg}}{T_{Lg} - T_{Sg}}\right)\left[C_{sg}\left(T - T_{Sg}\right)\right]}}{\mathrm{C_{sc}(T - T_{Lc}) - h_{fc} + C_{\ell c}(T_{Lc} - T_{oc})}}$
$T_{Sc} \leq T \leq T_{Lg}$	$\mathcal{R}_3 = \dfrac{\mathrm{C_{sg}\left(T_{og} - T_{Sg}\right) + \left(\frac{T_{Sg} - T}{T_{Lg} - T_{Sg}}\right)\left[C_{\ell g}\left(T - T_{Sg}\right) + h_{fg}\right] + \left(\frac{T - T_{Lg}}{T_{Lg} - T_{Sg}}\right)\left[C_{sg}\left(T - T_{Sg}\right)\right]}}{\mathrm{C_{\ell c}(T_{Lc} - T_{oc}) + \left(\frac{T - T_{Sc}}{T_{Lc} - T_{Sc}}\right)\left[C_{\ell c}(T - T_{Lc})\right] + \left(\frac{T_{Lc} - T}{T_{Lc} - T_{Sc}}\right)\left[C_{sc}(T - T_{Lc}) - h_{fc}\right]}}$
$T_{Lg} \leq T \leq T_{Lc}$	$\mathcal{R}_4 = \dfrac{\mathrm{C_{sg}\left(T_{og} - T_{Sg}\right) + C_{\ell g}\left(T_{Sg} - T_{Lg}\right) + C_{\ell g}(T_{Lg} - T) - h_{fg}}}{\mathrm{C_{\ell c}(T_{Lc} - T_{oc}) + \left(\frac{T - T_{Sc}}{T_{Lc} - T_{Sc}}\right)\left[C_{\ell c}(T - T_{Lc})\right] + \left(\frac{T_{Lc} - T}{T_{Lc} - T_{Sc}}\right)\left[C_{sc}(T - T_{Lc}) - h_{fc}\right]}}$
$T_{Lc} \leq T < T_{oc}$	$\mathcal{R}_5 = \dfrac{\mathrm{C_{sg}\left(T_{og} - T_{Sg}\right) + C_{\ell g}\left(T_{Sg} - T_{Lg}\right) + C_{\ell g}\left(T_{Lg} - T\right) - h_{fg}}}{\mathrm{C_{\ell c}(T - T_{oc})}}$

Table A3. Thermodynamic parameters for some relevant reactions. Sources of data cited in Fegley, 2013.

Reaction j	ΔH°_{298} (J/mol)	ΔC_p (J/mol)	ΔS°_{298} (J/mol)	$\Delta V^{\circ}_{s,298}$ (J/bar)	$\mathcal{R}^{*}_{c}$	f_c*
1	89790	-4.745	162.325	-1.969	1.666	0.625
2	84790	-5.295	129.88	-3.703	0.382	0.276
3	132890	-14.455	160.485	-3.429	0.360	0.265
4	84890	-0.465	173.525	-1.924	1.403	0.584
5	79890	-1.015	141.085	-3.658	0.322	0.243
6	127990	-10.175	171.685	-3.384	0.303	0.223
7	157380	-5.66	332.15	-2.094	1.302	0.566
8	178480	-3.16	337.45	-3.832	1.302	0.566
9	147380	-6.76	267.27	-7.831	0.298	0.230
10	168480	-4.26	272.57	-7.300	0.298	0.230
11	243580	-25.08	328.47	-7.283	0.281	0.219
12	265080	-22.58	333.77	-6.752	0.281	0.219
13	73990	0.725	171.455	-1.909	1.928	0.659

Table A4. Gibbs energy and reaction enthalpy for reactions listed in the Appendix at high temperatures and 200 MPa total pressure. *Units for G and H are Joules per mol of carbonate in j^{th} reaction. #All solid phases at unit activity except a_{albite}=0.7, $a_{jadeite}$=0.1, $a_{anorthite}$=0.3 $a_{Ca\text{-}Ts}$=0.01, $a_{enstatite}$=0.5, $a_{diopside}$=0.1 $a_{ferrosilite}$=0.5

Reaction j	ΔG (200 MPa, 875°C)*#	ΔG (200 MPa, 975 °C)	ΔG (200 MPa, 1075 °C)	ΔG (200 MPa, 1175 °C)	ΔG (200 MPa, 1275 °C)
	ΔH (200 MPa, 875°C)	ΔH (200 MPa, 975°C)	ΔH (200 MPa, 1075°C)	ΔH (200 MPa, 1175°C)	ΔH (200 MPa, 1275°C)
1	-18153	-28461	-38841	-49289	-59803
	86747	86273	85798	85234	84849
2	-1366	-10124	-18958	-27864	-36841
	81279	80749	+80220	79690	79691
3	-9345	-23650	-38103	-52697	-67424
	121574	120128	118683	117237	115792
4	-39651	-51060	-62505	-73987	-85506
	85494	85447	85401	85354	85308
5	-22870	-32728	-42628	-52568	-62551
	80025	79924	79822	79721	79619
6	-30843	-46248	-61767	-77395	-93127
	120320	119303	118285	117268	116250
7	-74763	-96172	-117693	-139322	-161058
	154557	153991	153425	152859	152293
8	-54529	-76120	-97804	-119575	-141437
	177787	177471	177155	176839	176523
9	22375	9197	-4099	-17513	-31041
	143620	142944	142268	141592	140916
10	-20965	-39457	-58050	-76740	-95528
	166850	166424	165998	165572	165146

11	-67999	-98738	-129745	-161004	-192505
	224211	221703	219195	216687	214179
12	7596	-18153	-44148	-70376	-96829
	247841	245583	243325	241067	238809
13	-47367	-58403	-69466	-80556	-91676
	75608	75680	75753	75825	75898

Table A5. Enthalpy per kilogram of carbonate reactant for reactions listed in Appendix

Reaction j	Reactant Carbonate	Reaction enthalpy per kg of carbonate reactant at 925 °C, 200 MPa
1	$CaCO_3$	864 kJ/kg
2	$CaCO_3$	809 kJ/kg
3	$CaCO_3$	1207 kJ/kg
4	$MgCO_3$	1014 kJ/kg
5	$MgCO_3$	949 kJ/kg
6	$MgCO_3$	1421 kJ/kg
7	$CaMg(CO_3)_2$	837 kJ/kg
8	$CaMg(CO_3)_2$	963 kJ/kg
9	$CaMg(CO_3)_2$	777 kJ/kg
10	$CaMg(CO_3)_2$	904 kJ/kg
11	$CaMg(CO_3)_2$	1209 kJ/kg
12	$CaMg(CO_3)_2$	1338 kJ/kg
13	$FeCO_3$	653 kJ/kg

Table A6. Values based on reaction 1 in text for which, by stoichiometry, $\mathcal{R}_c^* = 1.666$. Inasmuch as most other typical reactions exhibit larger endothermic reaction enthalpies, limits based on reaction 1 are conservative; other reactions would decrease the assimilation potential by requiring higher carbonatite to wallrock mass ratios to achieve a given temperature.

Temperature range	h(T) equations		Mixing ratio range for defined temperature limits	Mass fraction range of carbonatite for defined temperature limits
	granite	carbonatite		
$T_{og} \leq T \leq T_{Sg}$	eq (A14b)	eq (A7)	$1.09 \leq \boldsymbol{\mathcal{R}} \leq 1.802$	$0 \leq f_c \leq 0.646$
$T_{Sg} \leq T_f \leq T_{Sc}$	eq (A15b)	eq (A7)	$1.802 \leq \boldsymbol{\mathcal{R}} \leq 2.311$	$0.646 \leq f_c \leq 0.698$
$T_{Sc} \leq T_f \leq T_{Lg}$	eq (A15b)	eq (A6)	$2.311 \leq \boldsymbol{\mathcal{R}} \leq 15.53$	$0.696 \leq f_c \leq 0.940$
$T_{Lg} \leq T_f \leq T_{Lc}$	eq (A16b)	eq (A6)	$15.53 \leq \boldsymbol{\mathcal{R}} \leq 38.2$	$0.940 \leq f_c \leq 0.974$
$T_{Lc} \leq T_f \leq T_{oc}$	eq (A16b)	eq (A5)	$38.2 \leq \boldsymbol{\mathcal{R}} < \infty$	$0.974 \leq f_c \leq 1$